3-14-2006

Printing studies with conductive inks and exploration of new conducting polymer compositions

Anupama Karwa

Printing Studies with Conductive Inks and Exploration of New Conducting Polymer Compositions

Anupama Karwa

March 2006

Thesis submitted in partial fulfillment of the requirements for the degree of
Master of Science in Materials Science and Engineering

Approved:

_____

Dr. Thomas W. Smith (Advisor)

Accepted:

_____

K. S. V. Santhanam (Department Head)
Center for Materials Science and Engineering.
Rochester Institute of Technology
Rochester, New York 14623

Copyright Release Form:

I, Anupama Karwa, hereby grant permission to the Wallace Memorial Library of Rochester Institute of Technology to reproduce my thesis in whole or in part. Any reproduction will not be for commercial use or profit.

_____

Anupama Karwa

March, 2006

Table of contents

Thesis Statement:

Characterization of printed patterns using high volume printing processes; and exploration of options for the use of conductive polymers in inks for flexible printing and printable electronics.

Abstract:

In addition to low cost and high volume, continuous production of devices such as transistors and RFID tags, printable electronics show promise in the fabrication of a multiplicity of sensors, displays, photovoltaic arrays, smart cards, etc. Due to flexibility and insensitivity to substrates, the use of organics in printed electronics has opened up a number of new opportunities in novel applications.

In the present work, the process capability of flexography and offset lithography for patterning conductive materials was determined using small scale equipment (rotary letterpress and duplicator respectively). Process parameters including: type of substrate, line widths, line gaps, print thickness, directional effects, etc. were investigated. It was thus shown that the high volume printing processes of offset lithography and flexography can be used to obtain functional printed conductive patterns.

In order to have greater control over ink composition and physical characteristics than was afforded by commercially available silver metal filled conductive inks, polyaniline (PANI) was synthesized by interfacial polymerization. Printable flexographic inks were formulated therefrom and a PANI ink was used in the flexographic printing of a working gas sensor. The conductivity of these inks was lower than that of silver filled metallic inks. This mitigated their utility in their utility in the printing of functional RFID antennae.

Poly (thiophene-2, 5-diyl) (PT) and its derivatives are perhaps the most extensively studied class of conducting polymers and find applications in a variety of organic electronic devices. In the present work, an unprecedented approached to the synthesis and formulation of solution processible polythiophene (PT) compositions was explored. Conducting composites of polythiophene were synthesized by oxidative coupling of bithiophene, catalyzed by Fe^{3+} bound to the amphiphilic segment of functional block copolymers. Thus, amphiphilic block copolymers such as polystyrene-b-polyethylene oxide (PS-PEO) and polystyrene-b-polyacrylic acid (PS-PAA) complexed with Fe^{3+} were utilized as templates in the formation of soluble/redispersible prototype inks. The

distribution of the conductive phase is, in principle, determined by the morphology of the block copolymer. The composites were characterized by DSC, UV-vis and IR spectroscopy. PT formed in the presence of these amphiphilic block copolymers was oxidised using suitable doping agents. The compositions however failed to exhibit significant conductivity.

A number of challenges must be overcome in order to realize the potential economic benefits of using organic polymers in large scale electronic printing applications. The conductivity of inks based on organic conducting polymers can be increased by increasing the overall volume fraction of the conductive entity. The adhesion of the PANI compositions on various substrates could be improved by addition of a binding agent at a level that does not adversely affect the conductivity of the inks. Opportunities afforded by a post treatment/curing step may be considered and explored. Lastly, the ink formulation parameters and printing process variables should be optimized.

Acknowledgement

This thesis is dedicated to my family, friends, teachers and well wishers.

I would like to thank my parents and family for their constant support, love and encouragement in every difficulty that I faced while I was so far away from them.

Dr. Bruce Kahn for introducing me to the exciting new field of printable electronics. His input of ideas was an unceasing source of energy to undertake this research.

A heartfelt thanks to Dr. Thomas Smith for his initial guidance during the summer project and then a constant torch in finishing this thesis.

I would like to express my gratitude towards Dr. Andreas Langner for his help with the course work as well as for all the things I learned from just being around him.

Dan Clark and other members of the PAL for making available the printing equipment and vital suggestions about the printing processes and Franz Sigg for his help in designing the lithography and flexography plates. Special thanks to Brenda Mastrangelo for her constant help in the academic activities.

Eastman Kodak company for their generous funding to carry out the process capability studies. Parelec and Precisia for their generous donation of the conductive inks used in this work.

I would take this opportunity to thank Xia Yu, my project partner.

My days at RIT are some of the most wonderful memories that I will always cherish all through my life.

List of Figures

List of Tables

Preface

This research is a combination of three different projects.

The initial research began with a focus on defining process capabilities for high volume printing processes, flexography and offset lithography, and evaluating their utility in printing patterns using conductive inks. Results from this study demonstrated that conductive antennae that could be used in simple electronic applications can be reliably printed by flexographic or lithographic processes. Given this demonstration, a new dimension was given to the project.

In order to leverage numerous advantages of organic conductive polymers in printable electronic devices, the next phase was designed to explore processible conductive polymer compositions. This new dimension has two aspects, both involving research on the synthesis and formulation of organic ink systems using conducting polymers. Due to the extreme printing conditions of the lithography process, the rheology, printing and transfer characteristics and properties of litho inks must meet very stringent requirements. The inks must have high viscosity (pasty), oleophilic characteristics and must be shear thinning at high shear rates in order to accommodate splitting of inks on the rolls. They must also be designed to be used in conjunction with water based fountain solutions that render the non-image areas of the plate non-receptive for the inks. Accordingly, these inks must not emulsify in presence of the fountain solutions. It is difficult to obtain organic based inks meeting such requirements. Therefore this research was focused on developing model inks for flexography. In the first of these two aspects, polyaniline (PANI) nanofibers were synthesized by interfacial polymerization and printable flexographic inks were formulated therefrom. In the second, an unprecedented approached to the synthesis and formulation of solution processible polythiophene (PT) compositions was explored using template polymerization.

The entire work has therefore been divided into 3 broad Parts. The 1st part highlights work carried out towards defining printing process capabilities. The 2nd part highlights work related to obtaining the printable PANI compositions. The 3rd part is a more

exploratory work that provides a new protocol for synthesis of re-dispersible conducting polymer composites.

The global scope of this thesis is therefore the integration of various printing principles with the synthesis, formulation and characterization of conducting organic polymer systems. The study discloses two novel approaches to printable inks based on polyaniline nanofibers and polythiophene block copolymer composites.

Part A: Process Capability Studies Using Conductive Printed Patterns.

Introduction:

An Overview of Conventional Patterning of Electronics

Patterning of electronics to obtain specific designs is conventionally carried out on silicon wafers by photolithography. This is a process of transferring images and patterns from a mask to the surface of a silicon wafer. The steps typically involved in the photolithographic process are: wafer cleaning, barrier layer formation, photoresist application, soft baking, mask alignment, exposure and development and hard-baking.

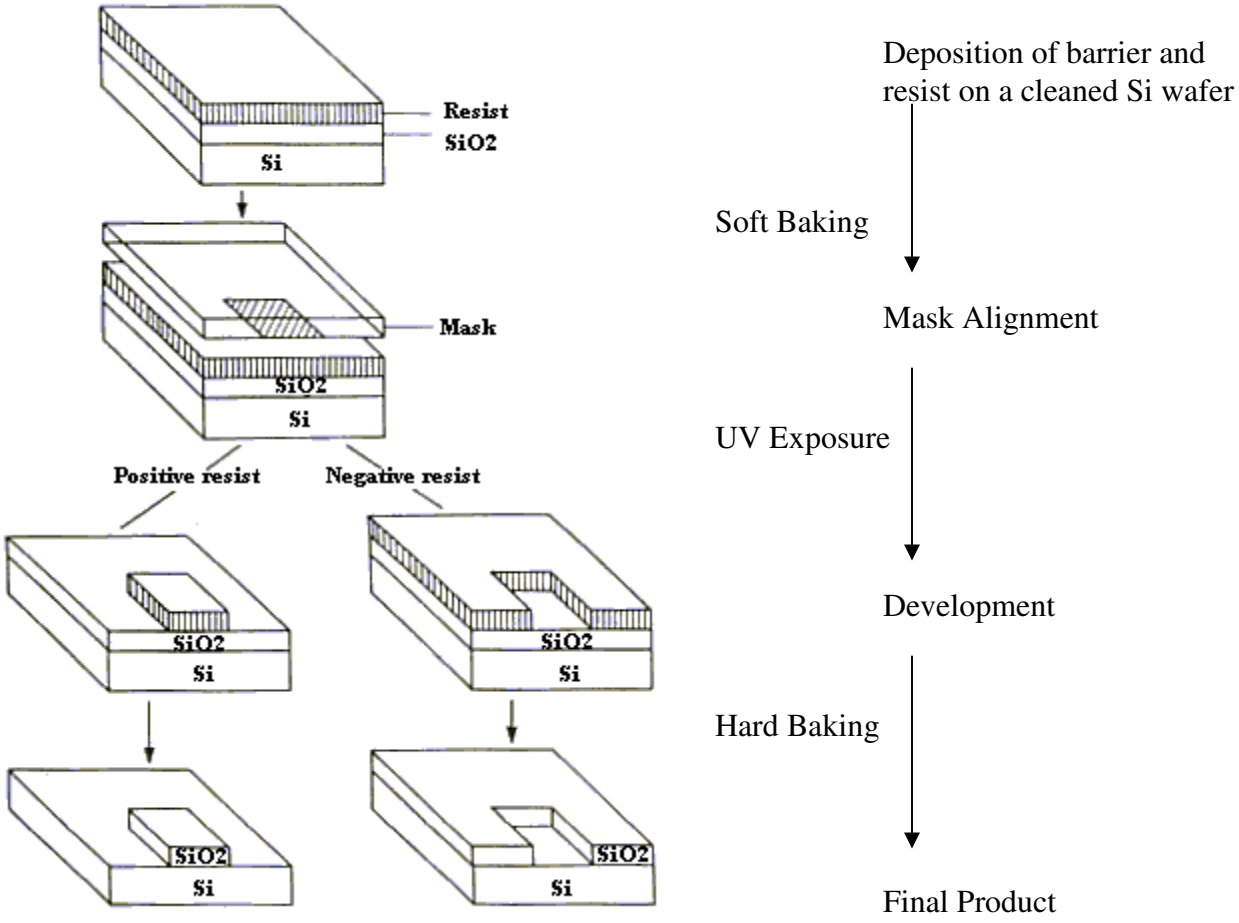

Figure 1: Conventional Silicon Processing
(http://www.ece.gatech.edu/research/labs/vc/theory/photolith.html)

The basic process is illustrated in **Figure 1.**

The silicon wafers are 1st chemically treated in order to remove particulate matter,

organic contaminants, and ionic and metallic impurities. Next, a passive silicon oxide barrier layer is grown across the surface of the wafer. A layer of either a positive or negative photoresist is then applied by spin coating. Soft-baking plays a very critical role in photo-imaging. In the soft-baking step, most of the solvent is removed from the photoresist coating. This photoresist layer is then covered with an appropriate mask and is exposed to actinic radiation. After photo-exposure and post exposure bake, the resist is developed by a selective solvent to reveal a negative or positive image of the pattern on the mask. (Positive: exposed material is removed, negative: unexposed material is removed). In the final step, the wafer is hard-baked in order to remove residual solvent from the photoresist and improve adhesion of the photoresist to the wafer surface. The resist protects the surface of the wafer and allows selective etching, doping, ion-implantation or metallization. Recent improvements and technological advances in the field of photolithography have made it possible to obtain circuitry of near nanoscale dimensions. [1].

Photolithographic patterning requires a large infrastructure. The industry however is well established and has benefited from continuing improvements in pattern resolution. Photolithography is used in the production of our most important electronic components, integrated circuits and devices.

While it is a complex, expensive and capital intensive process, given economies of scale ever lower cost microelectronics have been realized. Electronic circuits and devices patterned on crystalline silicon are, however constrained by limitations of wafer size. Accordingly this process on silicon does not lend itself to wide format applications like those in which novel plastic semiconductive materials can be leveraged [2]. Increased research in the field of printable electronics is being conducted because lithographic processes must accommodate serious environmental hazards like acidic and high heavy metal content effluents and use of volatile organic compounds (VOCs) in photoresist developers [3]. The environmental impact of photolithographic process is significant. The overall processing and development of photolithographic patterns consumes much more material than that contained in circuits and devices produced thereby [4].

The disposal of circuit boards is also a problem. Resin laminate substrates can contain fungicides, fire retardants and organic compound and toxic residues from soldering operations. These constituents necessitate recycling operations and disposal [5].

A Brief Introduction of Printed Electronics

Printed electronics may employ any of a number of printing technologies or processes to create electronic circuits and devices and electrical components and interconnects. Printed electronics can be used alone or in combination with conventional microelectronic components such as silicon chips for a range of different applications. Printing technologies have received increased interest recently because of their ability to pattern a variety of functional materials. Printing technology also allows use of various types of substrates including flexible media. Materials as varied as conductive and semi-conductive electronically functional polymers can be patterned using printable technologies. Direct printing of electronic features may create new markets and new low cost microelectronic products.

Today, there are a number of low resolution circuits and electronic devices that can be produced by printing. This field is opening up a wide array of novel applications that could be commercially and economically feasible in the future. The key is to make it efficient and affordable. Printing offers unique features including:

1) Customization in volume production
    - Short time cycle from design to manufacturing
    - Fast manufacturing runs
    - Reduced logistics costs
2) Production advantages
    - Ergonomic user interface solutions
    - Environmentally friendly
3) Applicability in novel products
    - Flexible structures
    - Low end integrated electronics [6]

Printing may be the optimum process for production of many plastic based electronic circuits, large area devices, and flexible electronics. Printing enables the production of disposable, thin and wearable electronics. Some of the interesting end applications for

printable electronics are identification, antennas, displays, RFIDs, sensors, batteries, security devices and quality indicators. Among the unique characteristics of printable electronics are that it has a low environmental impact, low cost, and may be the optimal process for production of disposable devices, single use devices, smart packaging, flexible electronics and large area devices [7].

Techniques and processes that have been explored in regard to their utility in printed electronics are: ink-jet printing, screen printing, flexography, lithography, spray printing, stamping etc. The majority of the work in this area has involved ink-jet [8] and screen-printing technologies [9]. The major high volume printing processes currently in use are offset lithography and flexography [3], [5], [10]. Printing of conductive inks to fabricate circuits [5], LEDs [11], sensors [12], microwave integrated circuits (MIC) [13], radio frequency circulator components on a wide range of flexible materials [14] etc. have been reported using offset lithography. Conductors, resistors, anodes/emitting layers, OLEDs [15] have been fabricated using flexography and gravure printing.

Key requirements for printable electronics are: need for functional fluid materials to build logics, a suitable high-speed and large volume printing process that makes ease of production and low cost feasible and adaptation to the process to print electronics

The key benefit of printed electronics is that it offers the possibility of using electronics in applications where the cost of silicon would make it impossible or the brittleness of silicon would make it inadequate [16]. In fact, this can be looked upon not as plastic-based microelectronics replacing the silicon industry but as building a different low-end commercial application industry. When conventional components are too big to be included in the silicon chip, it becomes uneconomical to increase chip sizes. Separate components add cost and failure modes. For such applications, printing seems to be the appropriate technology to explore [17].

Utility of High Volume Printing Processes in Printable Electronics

Extensive research has been carried out in printable electronics in ink-jet and screen-printing technologies. However, screen and ink-jet printing are relatively slow, limiting their productivity and use in high volume manufacturing [8]. A number of "soft lithographic" techniques have been used to make devices like transistors, RFID tags, wearable electronics and other novel applications [18], [19]. They too are however slow and have a limited production volume. Some of the major advantages of high volume printing processes are:

- High volume, high speed
- Additivity
- Substrate latitude (including flexible substrates)
- Large area printing
- Demonstrated repeatability
- Negligible waste
- Commercial availability of functional materials and infrastructure
- Utility in short run lengths
- Quick changeover/make ready systems

There are however some challenges. The following properties have to be appropriately optimized for offset lithography and flexography.

- Particle sizes distribution in the inks
- Solvent evaporation rate
- Rheological properties
- Substrate surface energy
- Printing speed

The major high volume printing processes explored in this work are offset lithography and Flexography. These two important printing processes are discussed briefly below along with the ink considerations for such processes.

1) Lithography

Lithography (or offset lithography) is a process that relies on two dissimilar wetting characteristics to produce an image. It may use photographic processes to make negatives. A schematic of the process can be seen in **Figure 2**

The plate making process: The lithography plate is a flexible aluminum or plastic printing plate. Modern printing plates have a brushed or roughened texture and are covered with a photosensitive emulsion. A photographic negative of the desired image is placed in contact with the emulsion and the plate is exposed to light. After development, the emulsion shows a reverse of the negative image, which is thus a duplicate of the original (positive) image. The plate is then chemically treated so the positive image is receptive to printing inks. The plate is affixed to a drum on a printing press. Rollers apply water (in form of the fountain solution), which wets the non-image areas of the plate, and ink, which adheres to the positive image areas. If this image were directly transferred to paper, it would create a positive image, but this would wet the paper as well. Instead, the plate rolls against a drum covered with a rubber blanket, which squeezes away the water and picks up the ink. The paper rolls across the blanket drum and the image is transferred to the paper. Because the image is first transferred, or offset to the rubber drum, this reproduction method is known as offset lithography or offset printing.

The advent of desktop publishing made it possible for type and images to be manipulated easily on personal computers for eventual printing on desktop or commercial presses. The development of digital imagesetters enabled print shops to produce negatives for platemaking directly from digital input, skipping the intermediate step of photographing an actual page layout. The recent development of the digital plate-setter eliminates film negatives altogether by exposing printing plates directly from digital input. [20]

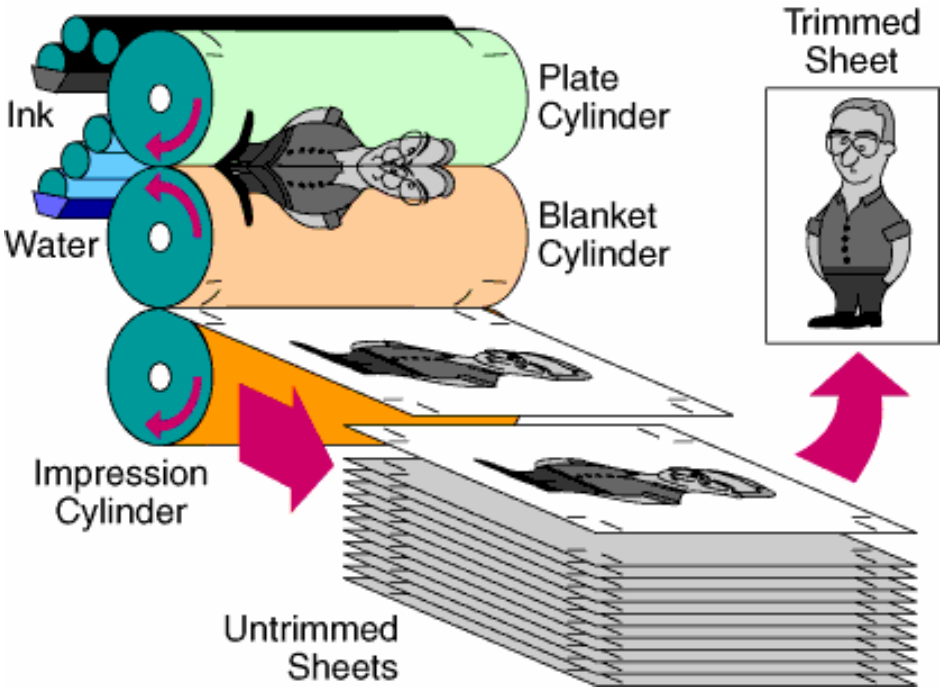

Figure 2: Schematic of a Lithographic Printing Process (http://www.bobs.co.uk/print/Offset.html)

The pros: This process has excellent control of registration and resolution in printing of circuit patterns. The commercial printing presses can be used for printing electronics. Conductive lithographic inks are also commercially available. Low ink volume is required for any given pattern. With the advent of waterless/UV inks, there is a substantial development potential in lithography. Waterless lithography makes use of purely of the difference of surface energy of the image area and non-image areas for ink transfer to image areas. With current printing developments, circuit components of up to 25 μm lines/gap have been achieved and thinner lines/gaps are being aimed for.

The cons: Offset lithography has a very high start up costs. The single printed ink layers are very thin (~1 micron). This makes multiple passes imperative especially in obtaining sufficient thickness for conductivity in ink films. The Start up waste on very short runs is high. The lithographic process requires stringent control on the ink rheology. Thus the inks have to be highly viscous. Therefore most available commercial inks are resins loaded with conductive materials like silver/copper particles or flakes or carbon black. It is difficult to formulate organic inks meeting such requirements [21]. Also ink drying speed and water balance in the printing process have to be optimized well.

2) Flexography

Flexographic printing process is a rotary relief method of printing. A schematic of the process can be seen in **Figure 3**. It uses a printing plate made of rubber, plastic, or some other flexible material. Recently photopolymers are also being used to increase the resolution and lifetime. The image pattern is raised on the plate like the raised areas on a rubber stamp. The plate is attached to a plate cylinder so that it can print in a rotary fashion. Ink is applied to a raised image on the plate using an engraved roller called anilox. The anilox roller has small cells or wells all over its surface, which transfer a precise volume of ink. Excess ink is wiped off by a doctor blade before printing. This helps in depositing a controlled amount of the ink to the substrate. Only the raised part (image part) on the plate receives the ink and the pattern is transferred to the substrate by the pressure of the impression cylinder. Non-image areas are below the printing surface and do not reproduce. The thickness of the film can be adjusted by controlling the rotating speed and the pressure applied on the substrate.

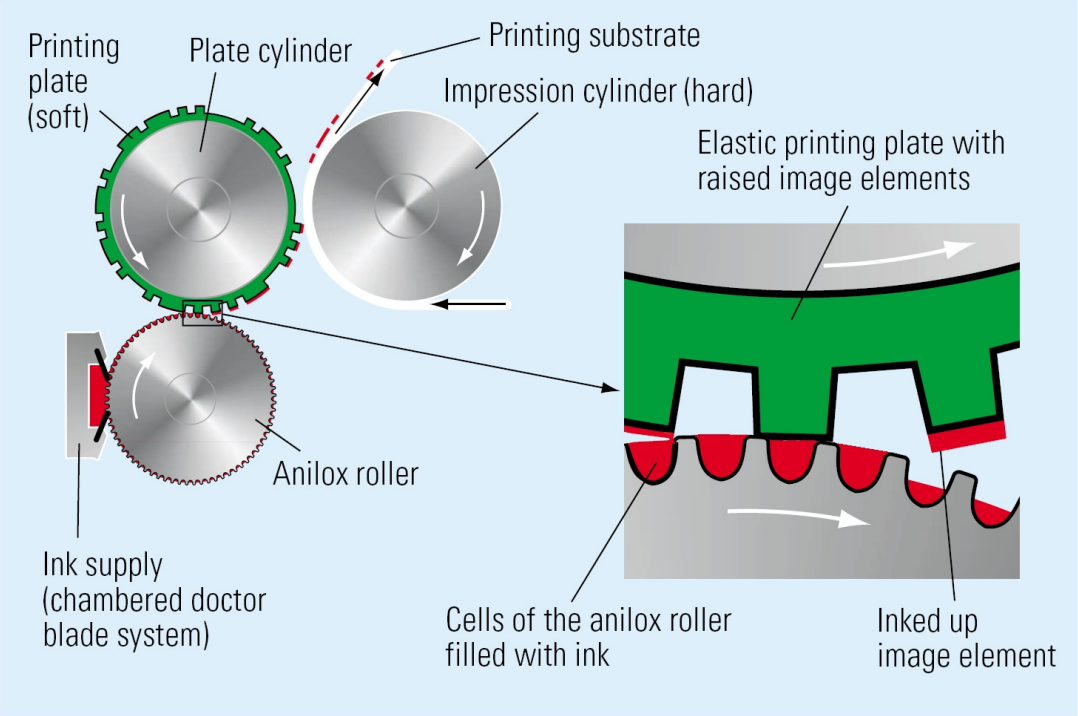

Figure 3: Schematic of a Flexographic printing process (H. Kipphan, Handbook of Print Media)

The pros: Flexography is a relatively easy and reliable process. The ink film thickness control can be a useful tool in obtaining uniform coverage over large areas. The fast-drying inks used in flexography make it ideal for printing on materials like plastics and foils. This makes flexography the predominant method used for printing flexible bags, wrappers, and similar forms of packaging. The soft rubber plates are also well-suited to printing on thick, compressible surfaces such as cardboard packaging. Inks used in flexography may be either water-based or solvent-based. [22] The process uses only a fraction of ink used in other techniques due to the anilox roll which meters ink quantities and the ink cures fully within hours. The process is relatively simple and convenient in that it exhibits excellent handling characteristics pre-press, on-press, and post-press. This process also shows tremendous room for development in improving results. Recently hard polymer capped plates or cushioned plates are being used to avoid dot gain (spread of ink out side of image areas due to squeezing of flexo plate during printing) or halo effects. The UV inks enable stop/start working, hence integration with in-line packing processes may be possible.

The cons: The raised image of the plate expands due to printing pressure leading to a gain in the image areas (dot gain). This leads to difficulty in registration and size monitoring. As can be seen below in **Figure 4**, one of the problems of flexography is the halo obtained around the actual printed edges. Due to this, only macro features are practically possible in flexography. Flexography can be used to print conductive traces, but the resolution obtained is limited.

Figure 4: Illustration of the Halo Effect in Flexography (Brian Brollier, International Paper)

3) Inks

The inks for the specialized field of printable electronics have to be specially designed. Both the intended application and the desired printing process will govern the composition of the ink. The physical properties of the wet ink are important in some applications but not in some others and similarly the physical properties of the dry ink film are important in some applications but not all. Identifying the function of a dry ink layer that is necessary to enable a desired application requires an understanding of the print process requirements and therefore the wet ink. The rheology and surface energy of inks determine the viscosity, applicable substrate, dry ink structure, adhesion, cohesion, and surface properties of the final print. The correct rheology of the ink depends not only on the intended printing process but also the specific printing equipment, ambient conditions, production speed and production parameters.

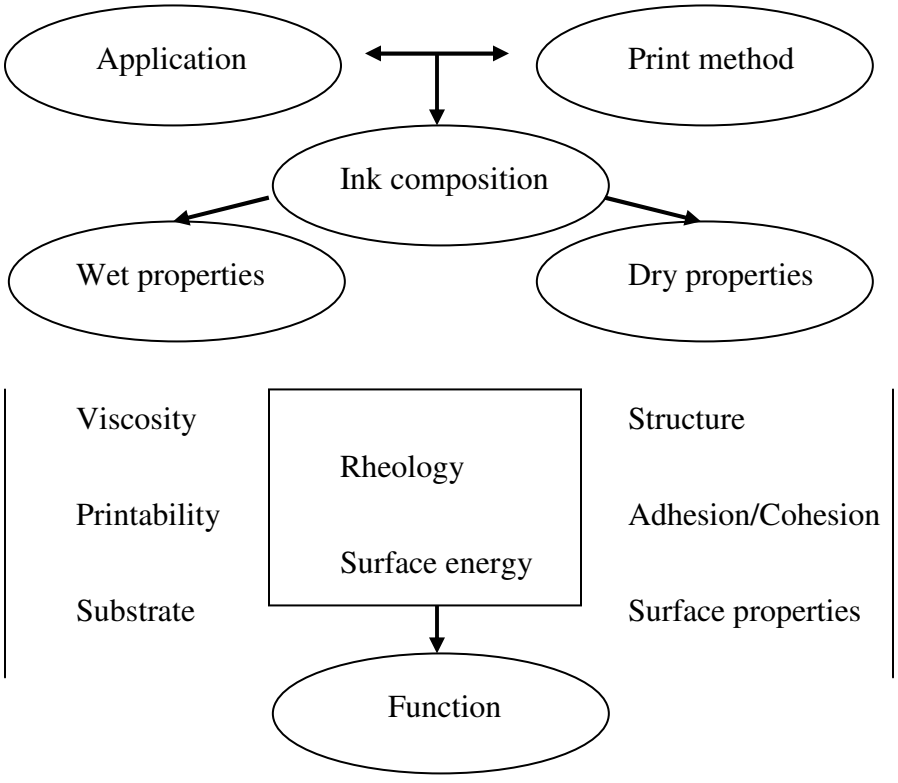

Figure 5: Various factors governing the properties of a conductive ink

There are a number of factors to be considered when formulating a specific ink (for both polymeric and metal particles filled inks) (**Figure 5**).

- Methods and ingredients for making conductive inks
- Conductive polymers
- Silver and other metal particles
- Factors affecting ink performance
- Factors affecting conductivity

It is difficult to correlate the rheological data collected under very controlled conditions with a printing process. The printing speed, scale, geometry, press setting, substrate, chemical contaminants etc. make it difficult to analyze the exact working conditions. Shear rates can be significantly higher in printing processes than in a rheometer. Thus indirect correlation is sometimes necessary to deduce projected behavior when transitioning from lab to press. Properties of the dry ink are also important to the functionality of a device constructed from electronic inks. Tests like adhesion, rub resistance and solvent resistance provide an indication of the robustness of the printed materials. However, due to variability in processes, applications and substrates, there are no well defined standard ranges for such properties [23].

Most commercially available conductive inks are comprised of finely dispersed conductive particles in a non-conductive resin matrix which bind the particles. The particles may be metallic copper, silver or aluminum or non-metallic conductive carbon blacks. The volume fraction of the conductive particles is generally maintained above the percolation threshold, the minimum volume fraction required for inter-particle connectivity. The inks may be used to produce conductive patterns on flexible and rigid substrates. The flexo/gravure inks are generally water-based and the litho inks are oil-based. Conductive inks are compatible with a variety of blankets, plates and substrates These inks have low volatile organic chemical content and are considered to be environmentally-friendly. Line resolution of 50 microns (2 mil) are achievable with the flexo/gravure inks, and 40 microns (1 mil) with the litho inks. The inks have sheet resistance as low as 100 Ω/□ at a film thickness of approximately 8 microns. For printed

resistors, ink formulations can be tuned to cover a wide range of sheet resistance (100Ω/□ – 500Ω/□) at a film thickness of 2 microns or less. [24]

The conductivity in a given ink formulation is governed by the printing process, drying method, substrate etc. The conductivity measurements are typically analyzed in terms of sheet resistivity (ρ_s)

$$\rho_s = \frac{\text{(resistance of a rectangular region of the printed conductor)*(width of region)}}{\text{(length of region)}}$$

The length of the conductive region divided by the width implies number of equal sided squares being measured. Hence sheet resistivity is reported in ohms per square (Ω/□).

Lithographic inks: These are highly viscous inks (paste inks). The tack or splitting of the ink between 2 rolls is an important property to be considered in multi-impression printing. Lithographic conductive inks must be designed such that they do not chemically dissolve in image or non-image areas on the printing plate. A common problem with lithographic inks is that splitting of ink filaments can lead to uneven texture. Inks should exhibit the phenomenon of "trapping". In this phenomenon, the first layer printed onto the substrate shows the ability to become more receptive to subsequent printed layers.

Flexographic inks: These are relatively low viscosity inks (fluid inks). Low viscosity is necessary because the ink needs to flow into the cells of the anilox rolls of the press. The inks must be designed to be readily re-dispersible over the lifetime of the product. Various dispersing agents and binders may be used to obtain optimum properties. [23]

Role of Organic Electronics in Low End Applications

Solid state integrated circuit processing combines multiple processes like masking, etching, evaporation, and deposition of materials under high vacuum. Printed organic electronics is an appealing technology, offering a processing window near or at atmospheric pressure and room temperature. [23] Printed organic circuits require up to 3 functional components: a conductor, a semiconductor and an insulator. π-Conducting polymers offer a unique combination of properties that make them attractive options in printed electronics. (**Figure 6**)

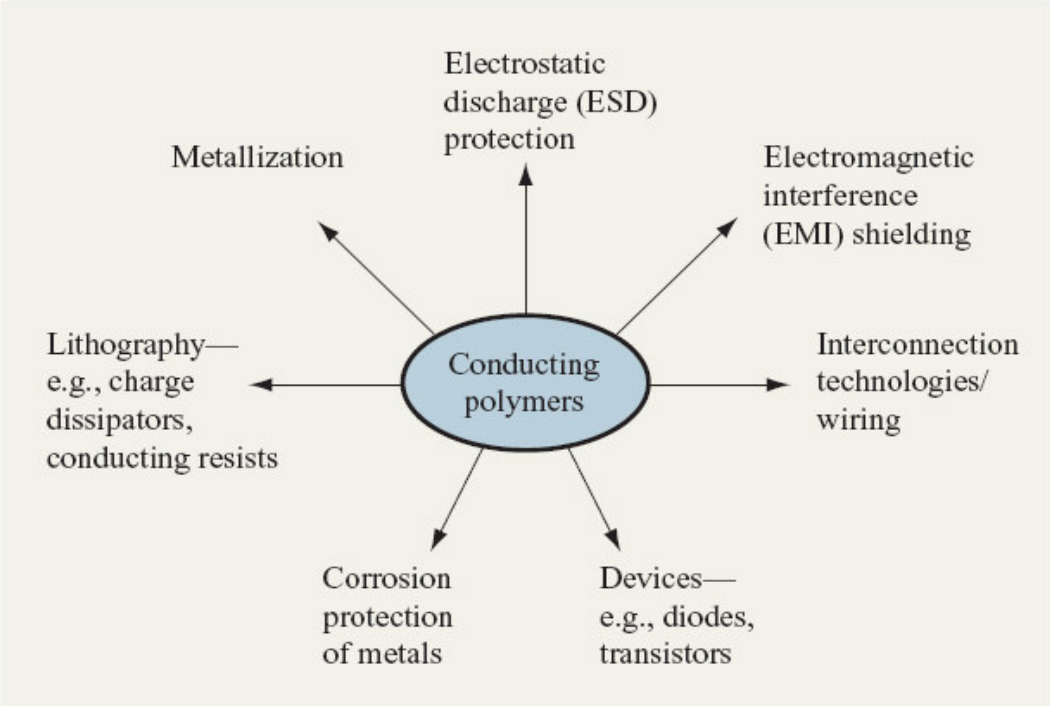

Figure 6: Overview of Some Potential Applications of Conducting Polymers in Microelectronics (M Angelopoulos, IBM J. Research and Development, 45, no. 1, (2001) pp 57)

Polymeric materials are flexible, lightweight and easily processed. π-conjugated polymers are generally made conducting by doping with an oxidizing agent, a reducing agent, or a protonic acid, to generate delocalized polycations or polyanions. The conductivity of these materials can be tuned by chemical composition, configuration and

conformation of the polymer backbone, by the nature of the dopant, by the degree of doping, and the volume fraction of the conducting polymer in the printing composition.

Conducting polymers can in principle be considered as candidates for interconnection technology. However, a dramatic enhancement of the conductivity of most processible and environmentally stable conducting polymers is required before they can be realistically considered as viable materials for interconnection technology. The use of conducting polymers in devices is another area that provides new technology in the future for IC fabrication and flat-panel displays. This is currently an active area of research. A number of resists based on conducting polymers have been developed. However, the performance of these systems is not currently at a stage that can compete with conventional resists. Significant improvements in resist resolution, contrast, and sensitivity are required. Conducting polymers are currently used for metallization of plated through-holes for printed circuit board technology. Conducting-polymer-based coatings have been developed that offer excellent electrostatic discharge (ESD) protection and numerous advantages over materials in current use. A number of the coating formulations are either already commercial or in the process of being rendered commercial. Corrosion protection of metals such as silver and copper using conducting polymers has also been shown to be quite promising. [25]

Process Capability Study

Introduction

The objective of the 1st part of the experimental work was the evaluation of the process capabilities of lithographic and flexographic printing processes for producing electrically conductive patterns. For this purpose, scaled down prototypes of machines representing the high volume printing processes of lithography (offset duplicator: **Figure 7**) and flexography (rotary letterpress: **Figure 8**) were used. Test patterns were designed specifically for this purpose. Commercially available conductive lithographic and flexo inks loaded with silver metal flakes were used to print the targets. The printed test patterns were characterized by profilometry, optical microscopy, and electrical measurements. A number of parameters were examined, including physical parameters (line width, thickness, space between lines) and electrical parameters (electrical conductivity, sheet resistance, longest electrically continuous path length, shorts between adjacent conductors, etc.) as a function of the printing conditions (number of impressions, registration, post treatment, substrate).

Figure 7: The Duplicator

Figure 8: The Rotary Letter Press

Results and Discussion

A number of test targets for the conductivity studies were designed by changing factors like line width, space width, incorporation of the electrode pads in the test patterns and the path length. A suitable test form was then designed and a series of experiments were conducted using offset lithography and flexography.

Lines (and spaces) of 42-126 μm for lithography and 169 μm for flexography were successfully printed. Electrical continuity was achieved for the 84 and 126 μm lines in lithography. The thickness of lines was found to lie in the range of 0.5 to 1.5 μm and increased with increase in number of impressions for lithography. Increasing the number of impressions improved the electrical conductivity. A maximum continuous conductive length of longer than one meter (including pads) and sheet resistivity less than 1 ohm/□ was obtained. It was found that a post treatment of heat and time aided in increasing the conductivity. An average decrease of about 25% in sheet resistance was obtained due to the post treatments.

The Lithography Test Target:

The design of the interdigitated test pattern is shown in **Figure 9**. Six patterns with line widths of 42μm, 84μm and 126μm, respectively in the vertical and horizontal orientations with respect to the printing direction were incorporated in one test form. Each pattern consisted of two continuous parallel lines with terminals marked as 1 and 2, respectively. The widths of the lines and the space between them were maintained the same. In order to assess the contribution of printing direction (horizontal or vertical) on the electrical results, the lines running horizontally on this test pattern were made thicker than the vertical lines. This way, the conductivity would be dominated by the lines running in the vertical direction and also the thick horizontal lines served as convenient pads for measuring the conductivity at intermediate positions along the test pattern. A total of 26 electrodes for every line were made including the two extreme terminals. By measuring adjacent electrodes along the same line, the resistance as well as the sheet resistance was

tested for short lengths of the lines. Short circuits could be easily detected and located by testing the resistance between two adjacent electrodes in different lines.

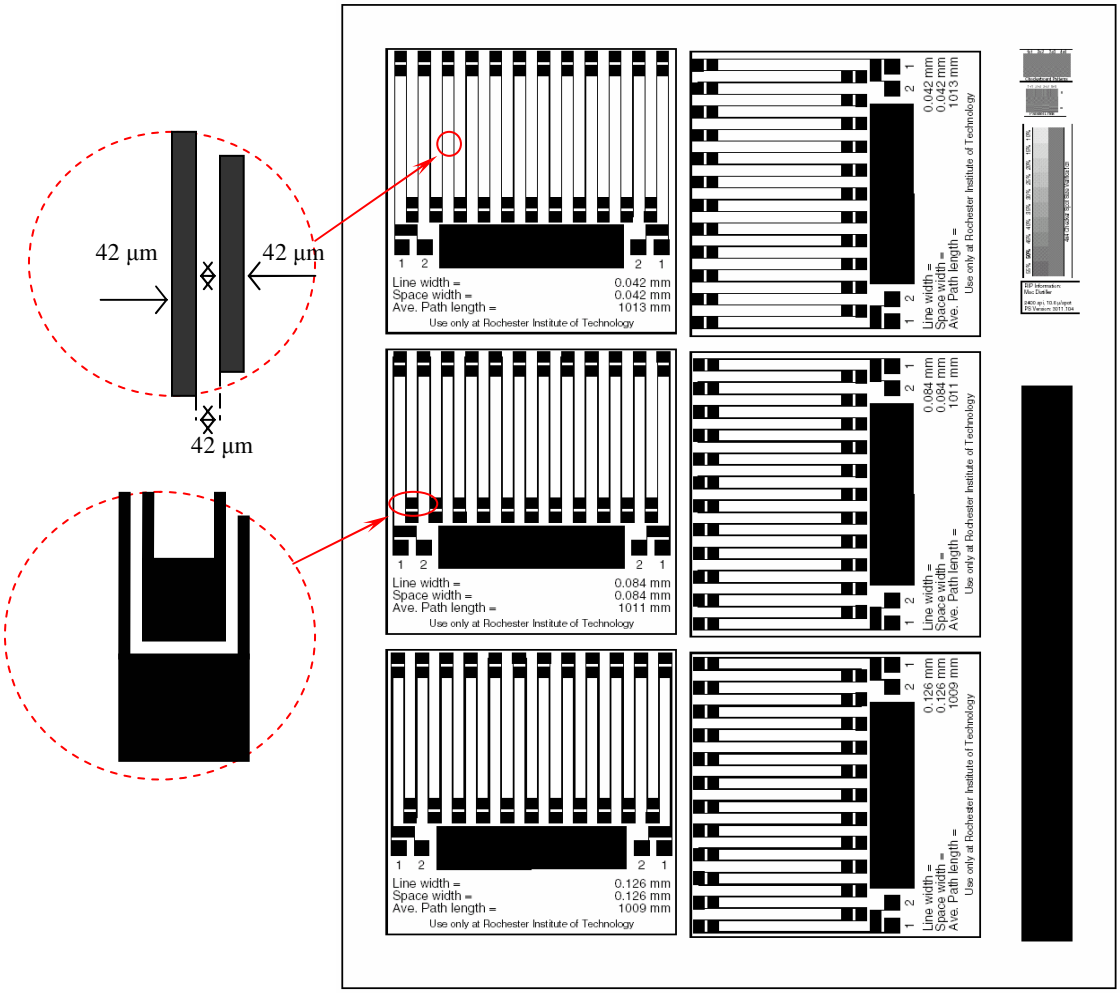

Figure 9: Lithography Test Target

The Flexography Test Target:

The design of the test pattern is shown in **Figure 10**. (a) A pattern with line width of 169 µm was used. The widths of the lines as well as the space between them are the same and are written below each pattern in the target. (b) Interdigitated pattern was designed from the point of view of a potential application. The line thickness is 1.974 mm and the space is 169 um.

The thick horizontal lines also serve as convenient pads for measuring the conductivity at intermediate positions along the test pattern. By measuring adjacent electrodes along the same line, the resistance as well as the sheet resistance can be tested for short lengths of the lines. Short circuits can be detected and located by testing the resistance between two adjacent electrodes in different lines.

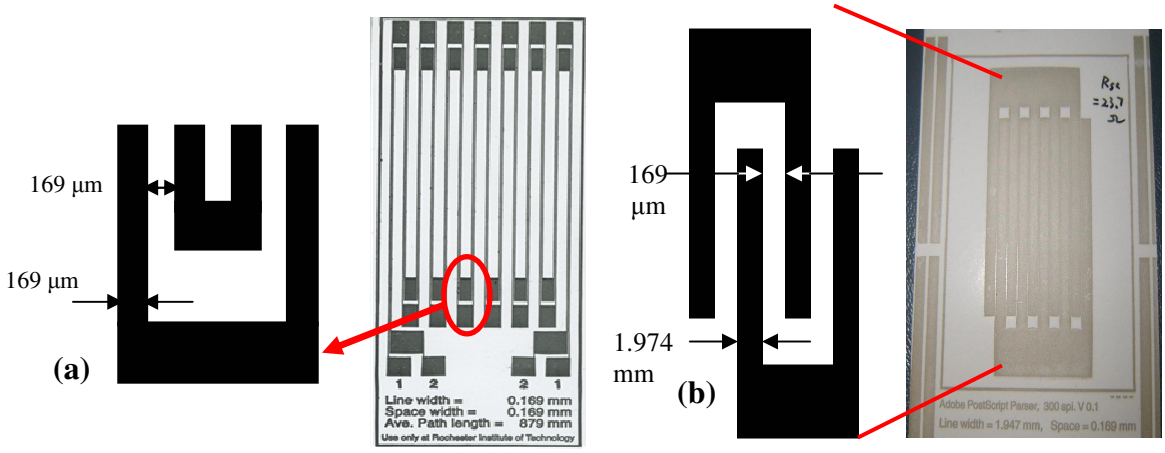

Figure 10: Flexography Test Targets

Resolution and Registration of images:

The two main characteristics that were tested in this study were the resolution of the image and the registration of the image.

Resolution: The degree of image sharpness that can be reproduced by a piece of equipment is termed as resolution. It is measured in dots per inch (dpi).

Registration: In printing, the fitting of subsequent colors or images in alignment with each other is termed as registration. Hence registration was studied for the multiple impression targets.

Line and Space Widths: Multi-Impressions:

Different line widths were printed having one, two and three impressions. Representative patterns with different line widths are shown in **Figure 11** which also shows lines printed

with different number of impressions. A minimum line width (as well as space width) of 42 μm was achieved while keeping the lines separate from each other.

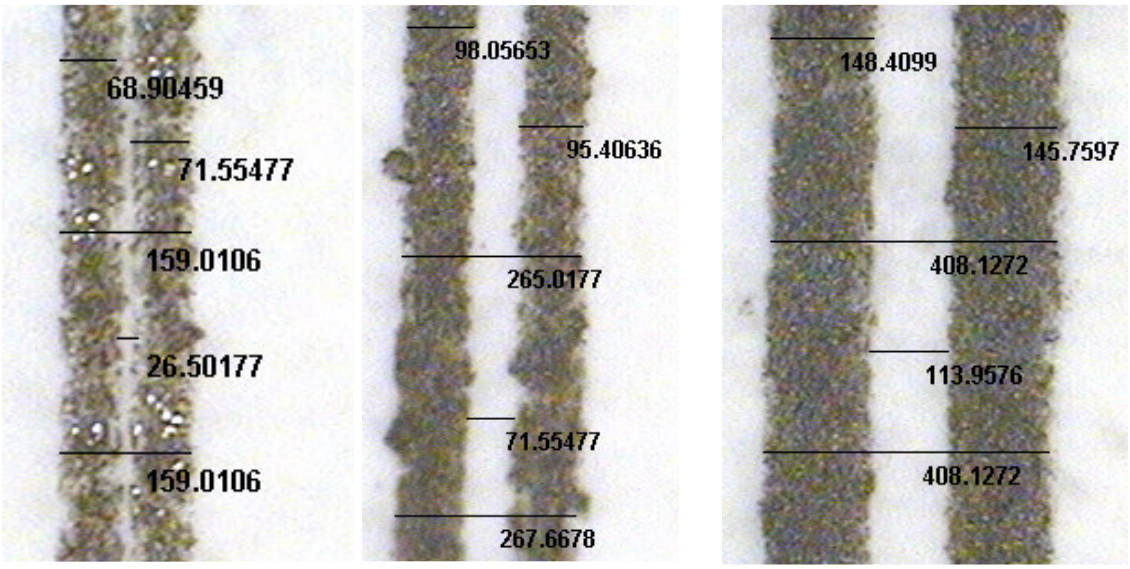

Figure 11: Optical Micrographs (120 X) of Printed Lines with Different Widths: the nominal line widths are (left to right) 42, 84, 126 um, respectively.

Line and Space Widths: Increase in Widths:

Table 1 shows the measured line widths as well as the percent increase from the designed (nominal) dimensions. These can also be seen visually in **Figure 12**. This increase is due to the dispersion of the ink during and after the printing. As apparent from table 1 and figure 13-14, the degree of increase is not proportional to the width of the pattern printed. The increase is quite constant when the designed width is relatively large. According to the working mechanism of offset lithography printing, the non-image part on the plate is hydrophilic which keeps ink away. Moreover, the lithographic ink is viscous and printed layer is only around 1μm in thickness. Therefore a smooth edge and limited amount of excess-printing are expected.

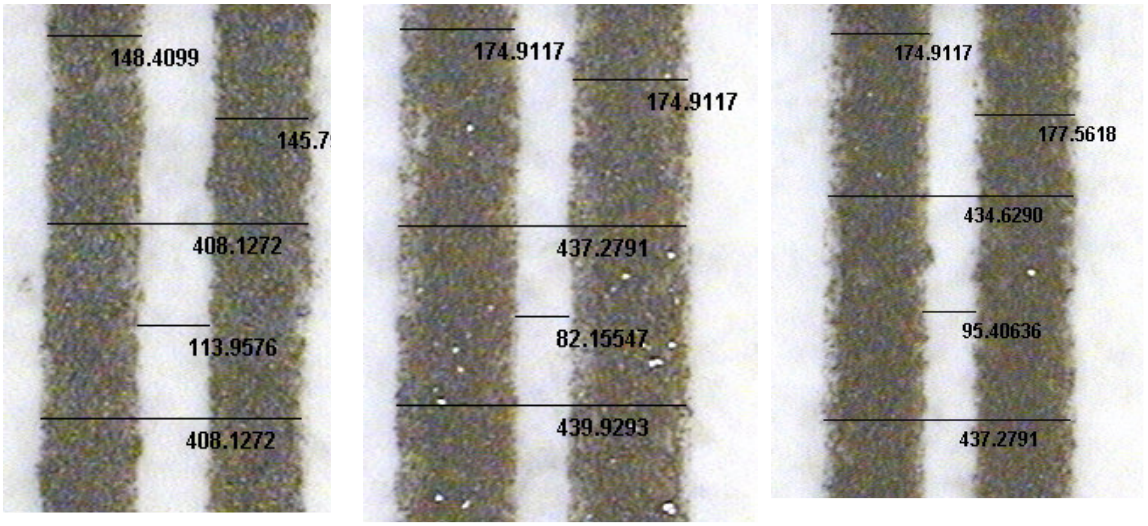

Figure 12: Different Number of Impressions: (left to right) one, two and three impressions for 126 um line.

Results Table		Line width					
		Vertical			Horizontal		
# of Impressions	Line width (μm)	Ave. Measured	Increase	% Increase	Ave. Measured	Increase	% Increase
1	42	69	27	64	83	41	98
	84	98	14	16	124	40	47
	126	147	21	17	167	41	33
2	42	70	28	67	78	36	85
	84	125	41	48	137	53	64
	126	175	49	39	169	43	34
3	42	72	30	70			
	84	135	51	61			
	126	176	50	40			

Table 1: Line Width and % Increase of the size

This information is shown graphically in **Figure 13 and Figure 14**

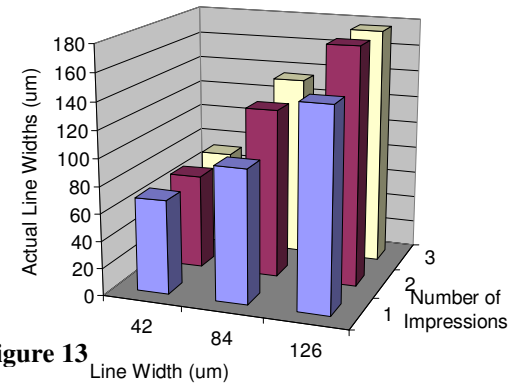

Figure 13

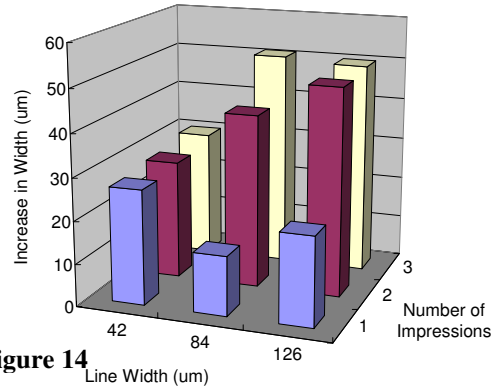

Figure 14

Figure 13: Actual Line Width Increase vs. Nominal Line Width and Number of Impressions

Figure 14: Absolute Line Width Increase vs. Nominal Line Width and Number of Impressions

Line and Space Widths: Directional Effects on Registration:

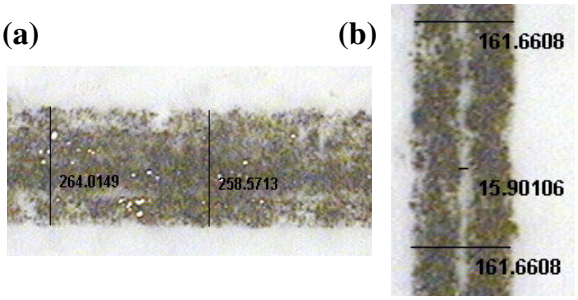

Figure 15: Optical Micrographs of 42µm Three Impression Printed Patterns a) Horizontal Direction (Poorly Aligned) b) Vertical Direction (Well Aligned)

An important factor that influences the line width is the printing direction. The horizontal sample is perpendicular to the direction of printing and to the direction of release of the substrate. This direction shows a larger line width increase than the vertical lines. It was observed that the registration in the horizontal direction was very poor as compared to that in the vertical direction. This can be seen from **Figure 15 a and b** where the three impression image printed horizontally shows worse registration as compared to the similar feature printed vertically. The corresponding space widths in relatively well aligned patterns and their decrease in spaces compared to the test target are shown in **Table 2**. It must be noted however that the multiple impressions were obtained by manually re-feeding printed substrates to obtain subsequent prints after drying of earlier

prints. The small-scale duplicator used had no mechanism to align the path of the substrate being fed correctly. Hence the observed decrease in the registration quality may be due to instrument limitations rather than process limitations.

Results Table		Space width					
		Vertical			Horizontal		
# of Impressions	Space width (μm)	Measured	Decrease	% Decrease	Measured	Decrease	% Decrease
1	42	24	27	64	27	41	98
	84	72	14	16	68	40	47
	126	147	21	17	167	41	33
2	42	70	28	67	78	36	85
	84	125	41	48	137	53	64
	126	175	49	39	169	43	34
3	42	72	30	70			
	84	135	51	61			
	126	176	50	40			

Table 2: Space Width and % Decrease of the Size

The major challenge in multilayer printing is the alignment accuracy of the subsequent layers of ink with the previous layers. As can be seen in the table and images, the best line resolution (minimum line width) was obtained for a single impression. The registration for the two and three impressions was not very good due to machine limitations. However, multiple layers increased the line thickness and hence the conductivity of the printed line. This factor should also be considered while fabricating complicated multi-layer electronic devices.

Line Thickness:

Table 3 shows the results of the line thickness for each of the samples. A stylus profilometry image of the line cross section is shown in **Figure 16**. Although the surface of these printed layers is quite rough, it can be seen that the line thickness increases with the number of impressions. However, **Figure 17 and Figure 18** show that line thickness increases by approximately 46% going from one to two impressions and by about 18% going from two to three impressions. This indicates that the rate of increase in line

thickness decreases with increase in number of impressions. This phenomenon can be explained as follows: The pressure between the blanket and impression cylinder increases due to increase in substrate height after the 1st impression (due to underlying ink layer). This leads to a relatively thinner layer. The patterns were dried between subsequent impressions. However the pattern might not be totally dried before a second layer printed on. Moreover, the silver particles in the newly printed layer fill up the gaps and pores in the underlying layers and hence contribute less to increasing the thickness. It is also observed that the thickness increases with line width.

		Thickness					
		Vertical (Average from five tests)			Horizontal		
# of Impressions	Line width (μm)	Line 1(μm)	Line 2	Average	Line 1(μm)	Line 2	Average
1	42	0.31	0.36	0.33	0.23	0.25	0.24
	84	0.66	0.69	0.67	0.20	0.55	0.38
	126	0.70	0.79	0.74	0.61	0.76	0.69
2	42	0.41	0.40	0.41	0.15	0.41	0.28
	84	0.97	1.02	1.00	1.08	0.44	0.76
	126	1.15	0.99	1.07	1.32	1.68	1.50
3	42	0.68	0.70	0.69			
	84	1.03	1.25	1.14			
	126	1.31	1.30	1.30			

Table 3: Line Thickness

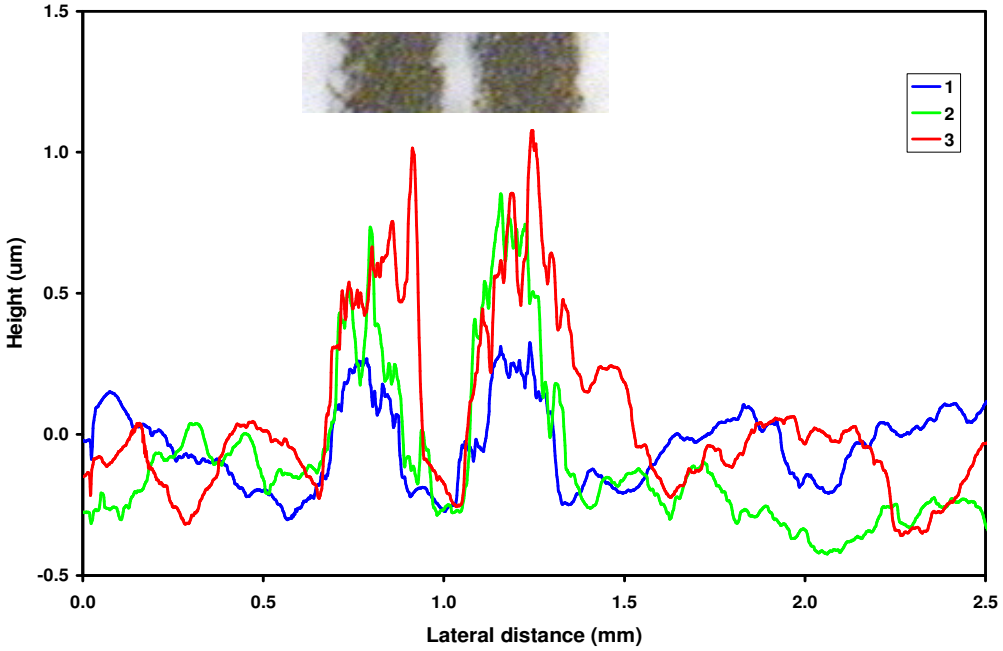

Figure 16: Profilometry vs. Number of Impressions

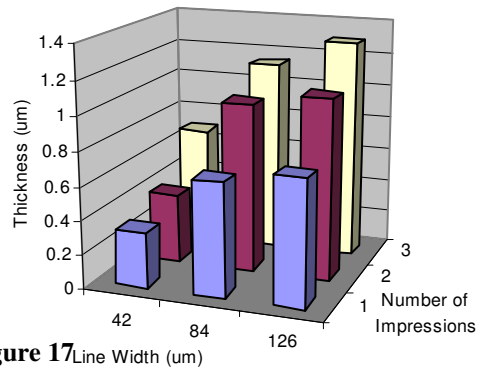

Figure 17

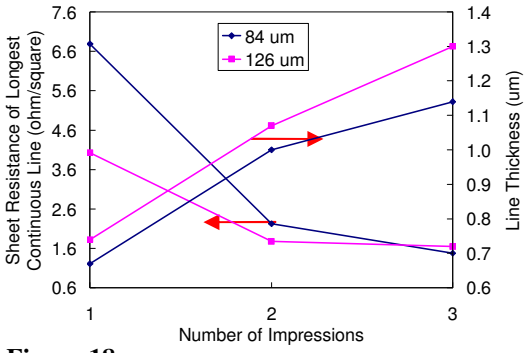

Figure 18

Figure 17: Line Thickness vs. Nominal Line Width and Number of Impressions

Figure 18: Line Thickness and Sheet Resistance Increase with Number of Impressions in 84 and 126 µm lines.

Conductivity:

The resistance of the lines (26 electrodes per line, two conductive lines per pattern, as shown in figure 9) was measured and the corresponding sheet resistance was calculated.

The results are shown in **Table 4** and **Figure 19 and Figure 20**. The maximum continuous conductive length obtained was about one meter (including pads). The lowest sheet resistivity along a distance of 551 mm is less than 1 Ω/□.

It was observed that the sheet resistivity of the samples decreased (conductivity increases) with the number of impressions. As is shown in **Figure 18-19**, there is a greater increase in conductivity (decrease in resistivity) going from one to two impressions than going from two to three impressions. This is because deposition of the second ink layer essentially fills up voids that are left in the first layer increasing the conductivity. Also, much of the first impression fills voids in the rough surface of the substrate (coated paper), and does not contribute as much to the conductivity as subsequent layers. This phenomenon is also exhibited in the results of the line thickness where the deposition of the second layer does not increase the thickness proportionally. The sheet resistance of the lines is essentially independent of the line widths. The continuous conductive length increases from 42 μm to 126 μm feature size in each sample and also with the number of impressions.

Results Table		Sheet Resistance (Using Actual Line Widths)							
		Vertical				Horizontal			
# of Impressions	Line width (μm)	minimum $R_{□}$	average $R_{□}$	standard deviation	longest continuous line(mm)/ $R_{□}$	minimum $R_{□}$	average $R_{□}$	standard deviation	longest continuous line(mm)/ $R_{□}$
1	42								
	84	5.98	7.04	0.82	77/6.79				
	126	2.59	4.36	0.99	192.5/4.03	4.58	8.20	4.05	77/5.58
2	42								
	84	1.34	2.62	0.50	500.5/2.23	2.11	2.91	0.36	934/2.89
	126	1.44	2.58	0.44	320/1.78	2.03	2.89	0.49	544/3.30
3	42	1.25	2.13	0.28	320/1.96				
	84	1.06	1.93	0.39	551/1.48				
	126	1.06	1.70	0.26	934/1.65				

Table 4: Resistance and Sheet Resistance of the Lines

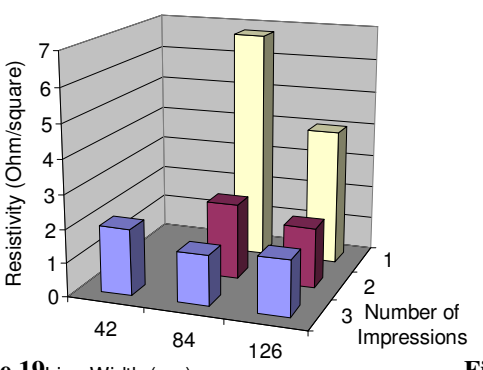

Figure 19

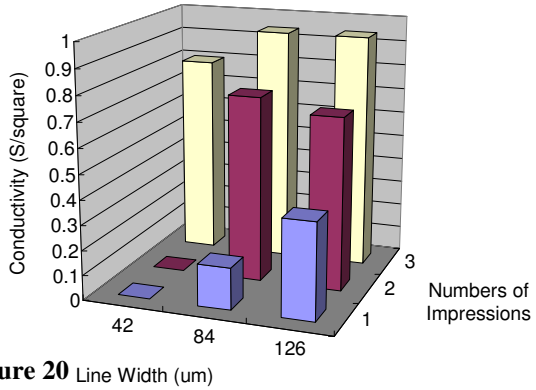

Figure 20

Figure 19: Line Resistance vs. Nominal Line Width and Number of Impressions

Figure 20: Line Conductance vs. Nominal Line Width and Number of Impressions

Effect of Heat Treatment on Conductivity:

An increase in the conductivity was observed in the printed ink surfaces with time and heat treatment. **Figure 21** shows the resistance of a sample (line width 84µm, horizontal printing, and two impressions) as a function of the curing conditions. **Table 5** gives the resistivity data for all the samples. This phenomenon is most likely due to drying of the ink (which may occur by a variety of mechanisms) which gives rise to improved packing of the silver particles with time. This causes a decrease in the resistivity (hence an increase in the conductivity). This process can be accelerated by high temperature treatment for a short time.

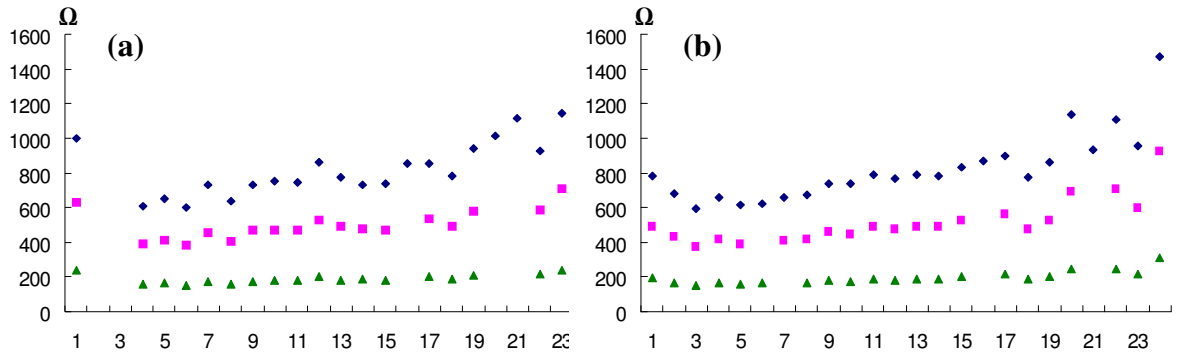

Resistance data for parallel printed lines (a) and (b) of a Sample (Line Width 84µm, Horizontal Printing, Double Impression). Blue diamonds are the original data, pink squares were tested after two weeks (room temperature) and the green triangles were heat treated at 130^{0}C for 10 mins and tested after sample cooled down to room temperature.

Figure 21: Effect of heat treatment and time on the resistance of a sample.

Line Parameters		84 um, double impression, horizontal	126 um, double impression, vertical	126 um, triple impression, vertical
Original	Lowest Ω□	2.11	1.44	1.06
	Average Ω□	2.91	2.58	1.70
	Standard deviation	0.36	0.44	0.26
	Longest continuous line(mm)/Ω□	934/2.89	320/1.78	934/1.65
After 2 Weeks	Lowest Ω□	1.34	0.85	0.68
	Average Ω□	1.85	1.52	1.10
	Standard deviation	0.28	0.27	0.17
	Longest continuous line(mm)/ Ω□	462/1.61	320/1.07	934/1.07
130 °c 10 min.	Lowest Ω□	0.54		
	Average Ω□	0.69		
	Standard deviation	0.07		
	Longest continuous line(mm)/Ω□	462/0.62		

Table 5: Change of Resistance with Curing Conditions

Flexography:

a) Registration: The edges of an originally straight pattern (indicated with black lines) was widened due to plate compression due to printing pressure in flexography as can be seen in **Figure 22**. This happens mostly due to squeezing ink out at the edges.

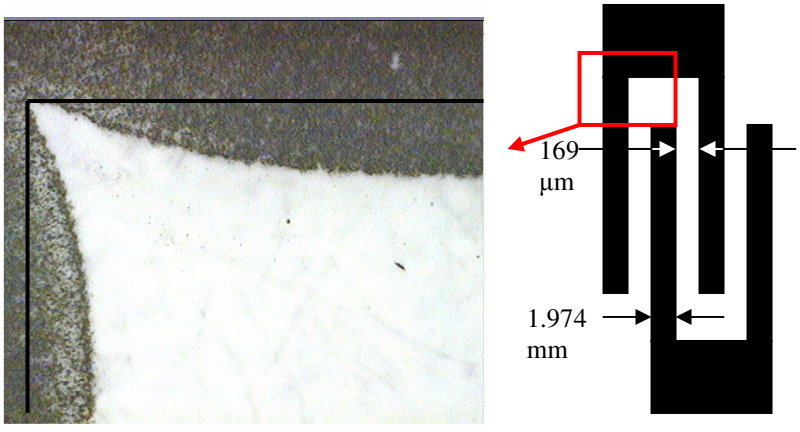

Figure 22: Rounding of edges due to pressure on flexo plate

b) Line Widths:

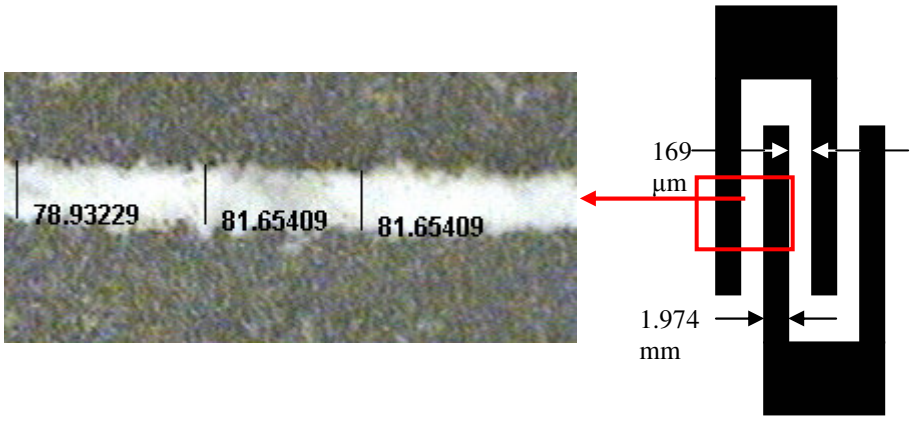

Figure 23: The space between the lines is much lower than that in the original plate design due to 'bleeding' of ink

Figure 23 shows an image displaying the width of the space between the lines. The original design on the plate is designed for a space width of 169 um. However due to 'bleeding of ink' from both sides the inked lines were much thicker and the spaces much thinner than the original design.

Flexo vs. Litho: Line Registration and Sharpness:

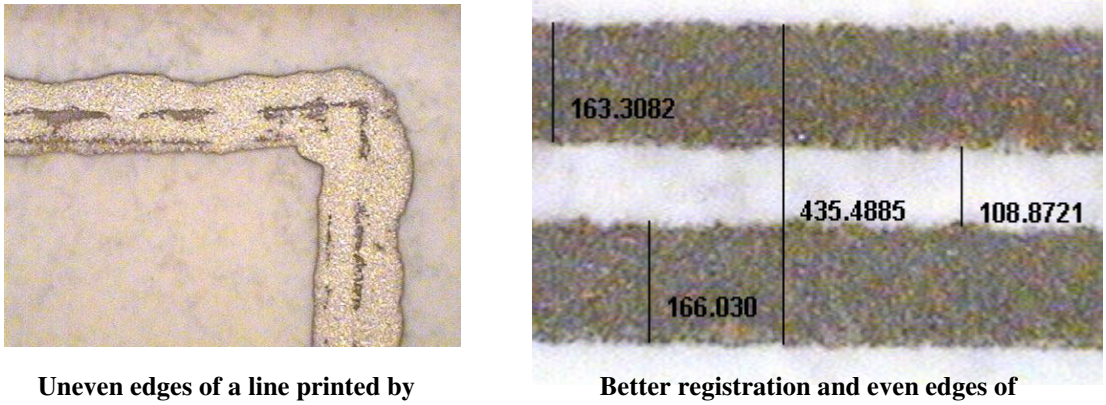

Uneven edges of a line printed by Flexography

Better registration and even edges of a line printed by Lithography

Figure 24: Registration of a line printed by flexography and lithography (left to right)

Figure 24 makes apparent the difference in the lines obtained by lithography which show a much better registration, sharper edges and a better control on the dimensions as compared to that shown by flexography.

Summary and Conclusion

The two high volume printing processes lithography and flexography were used to print patterns using conductive inks. Test targets were designed with variables like line width and space width. Electrode pads were also incorporated in the test patterns in the path length for testing purposes. Other parameters such as printing direction, curing, substrate and line thickness were studied for offset lithography.

Lines and spaces between lines from 42-126 μm were printed successfully. Electrical continuity was achieved for the 84 and 126 μm lines. The thickness of lines was found to lie in the range of 0.5 to 1.5 μm and increased with increase in number of impressions. Increasing the number of impressions improved the electrical conductivity. The thickness however did not increase proportionate to the number of impressions. A maximum continuous conductive length of longer than one meter (including pads) was obtained with sheet resistivity less than 1 Ω/□.

It was found that a post treatment of heat and time aided in decreasing the sheet resistance by approximately 20% of the initial value.

Test targets were obtained for antennas using commercial lithography inks by offset lithography. The targets obtained by flexography were successfully used in sensor fabrication.

Due to plate limitations and poor control over printing parameters, certain problems like bleeding of ink, poor registration and width gain were observed in both processes. These were more pronounced in flexography.

Experimental

The test targets were designed and programmed in PostScript. The PostScript code includes parameters to change the line widths and gaps to obtain the various targets in both the vertical and the horizontal orientations. The internal logic of PostScript adapts to the output device and gives the required resolution. The resolution used was 2400dpi was used for making the negative.

Lithography:

The test targets were written to Kodak Recording 2000 negative film at a resolution of 2400 dpi using an AGFA SelectSet 5000 Imagesetter. The film was developed using RA 2000 developer and Kodak RA 3000 fixer in a Dupont Easy Compact 95 Rapid Access Film Processor.

Enco aluminium plates covered with a UV sensitive photoresist polymer were used. These plates have a ridged/grained texture that helps to hold water on the non image areas during the printing process. These plates were exposed for 1.5 minutes in a 25 psi vacuum using a Nu-arc Ft32V3UP ultra-plus flip flop platemaker. They were developed using Enco ND-143 Negative aqueous developer, and finished using New Century Press Room Product-Plate Cleaner, Preserver and Finisher.

An Itek 960 Offset Duplicator press was used with R10 Conductive Ink Formula 2 (Precisia), and Anchor # 7039 ISO 99 fountain solution. The ink viscosity was determined to be 100 Pa.s at 10 rpm using a Brookfield viscometer. The equipment and rollers were cleaned after printing using Varn Wash V-120 and LBC Special General Purpose Cleaner from Danka Industries.

The substrate used was Sapp Lustro Coloss 100# text paper. Different numbers of impressions were obtained by feeding printed (and dried) patterns back into the duplicator.

Each sample was evaluated in both the horizontal (pattern lines perpendicular to the direction of printing) and the vertical (pattern lines parallel to the direction of printing) directions. The line widths used in the test patterns were 42, 84 and 126 μm.

To obtain two and three impression samples, single impression samples were dried after printing and some of them were fed into the duplicator again to receive a second impression. Following this second impression, the samples were dried again, and some of them fed into the duplicator for a third time.

Line thickness (height) measurement was carried out using a Tencor P2 profilometer, using the following conditions: 1000 μm scan length, 50μm/sec scan speed, 40 sec scan time, 50 Hz sampling rate, 1.00 μm horizontal (lateral) resolution, 300μm/25 Å vertical range resolution. Actual line widths were obtained using an Olympus BX60 optical microscope at 120X magnification and ImagePro (Media Cybernetics) image evaluation software. Electrical conductivity was tested using a Fluke 73 Multimeter.

Flexography:

The flexographic printing plates were designed in PostScript, and produced on DuPont Cyrel by Adflex Corporation. An IGT Rotary Letterpress (Specifications: Printing force 50-200 N: Printing speed 0.2-1.5 m/s). Polyaniline ink and commercially available conductive flexo ink CLO-101A (Precisia) were used for printing. The equipment and rollers were cleaned after printing using Varn Wash V-120 and LBC Special General Purpose Cleaner from Danka Industries.

The substrate used was Sapp Lustro Coloss 100# text paper. Electrical conductivity was tested using a Fluke 73 Multimeter.

Actual line widths were obtained using an Olympus BX60 optical microscope at 120X magnification and ImagePro (Media Cybernetics) image evaluation software.

Part B: Formulation and Evaluation of PANI Compositions.

Introduction

Semiconducting organic molecules and conjugated polymers exhibit various qualities like potentially low cost, solution-processibility, advantageous opto-eletronic properties, and other specific properties (such as color, luminescence etc) that may be harnessed in novel printing applications. Examples include self-assembled ordered structures with charge carrier mobilities close to that of thin film silicon for application in transistor circuits [18], light emitting diodes made from organic polymers because of their potential low cost and applicability to color flat panel displays [26], solar cells [27], and field-effect transistors [28], [29]

The organic inks show a considerably lower mobility, low switching speeds and high resistivity [30]. The manufacturing/production techniques need development. The high volume printing techniques need to be optimized for repeatability, printing speed, metered material deposition [30], [31], and pattern dimensions. The macro and micro structures of the printing ink and printed layers strongly impact device performance. Hence adequate research should be channelized towards study of ink materials, formulations, the pre and post treatments (if required), additives, and printed ink film qualities. Material properties must be optimized for the both the printing equipment as well as application requirements. Along with appropriate designing, there is also a need for establishment of standards/benchmarks for testing/characterization [31].

In the past, PANI was considered to be an intractable and insoluble polymer (at high molecular weights). In the recent years however, a number of reports have appeared describing the synthesis of PANI in more tractable, film forming compositons. Some of the methods that have been reported use various types of functionalized doping agents that improve the melt processibility and solution processibility of the polymer [30], [32], [33]. Other methods of garnering processibility include the use of specific solvents [34], [35], and template polymerization [36] to yield nanofibers, nanorods, nanotubes etc. [37]. PANI now stands out as one of the most studied, most processible and most robust conducting polymers. It is highly dispersible, environmentally stable, and easily synthesized in essentially one-step from inexpensive starting materials. The properties of

the polymer can be tuned to meet the needs of a given application. Today, as a result of chemical modification of the polymer backbone and doping to control the oxidation state, many conductive PANI derivatives have been reported [25].

Polyaniline (PANI) in its base form is non conducting and has a general structure depicted in **Figure 25**. The insulating half-oxidized emeraldine base (EB) form of PANI can be regarded as a copolymer of reduced and oxidized units, as is shown. EB consists, therefore, of phenylene diamine and quinoid diimine units.

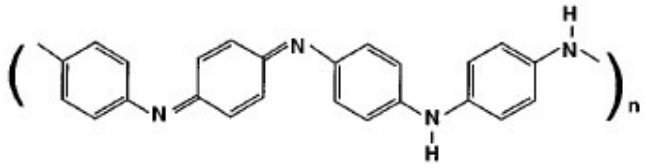

Figure 25: Emeraldine base form (non conductive form) PANI (J. Huang, et. al., Chem. Eur. J. 2004, 10, 1314-1319)

EB is generally doped with protonic acids such as aqueous hydrochloric acid (HCl) to give conductivity of the order of 1 S/cm^2. (**Figure 26**) The iminic nitrogens can be protonated by strong acids to form an acid-base complex, i.e., emeraldine salt, which is electrically conducting. The complex is a stable delocalized polysemiquinone radical cation. Due to a half-filled polaron band, the complex is electrically conducting.

EB is soluble in some hydrogen bonding solvents, such as sulphuric acid, 80% acetic acid, and N-methylpyrrolidone (NMP). The protonated PANI is, however, observed to be less soluble in these solvents. When bulkier counterions are used, the solubility is observed to increase. Moreover, solubility in weakly polar solvents is achieved when the protonating counterion simultaneously acts as a surfactant for the solvent. [35]

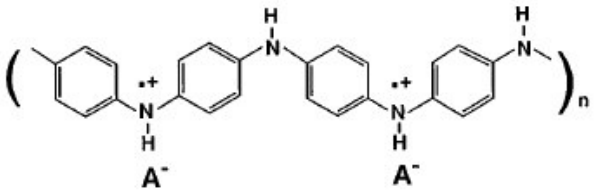

Figure 26: Emeraldine salt form (conductive form) of PANI ((J. Huang, et. al., Chem. Eur. J. 2004, 10, 1314-1319)

In recent years, one-dimensional (1-D) PANI nanostructures like nanowires, rods, and tubes have gained importance since they are advantageous in terms of both low-dimensional systems and organic conductors. Synthesis of such structures has been carried out both chemically and electrochemically by template polymerization. However, these methods are complicated and have tedious post processing steps and low yields.

Interfacial polymerization of aniline to obtain PANI nanofibers was used in this project. This method is a practical synthetic method capable of making pure, uniform, and template-free PANI nanostructures with small diameters (sub-100 nm) in bulk quantities. The method does not necessitate a need for any special dopant or solvent. The nanofibers produced by this method have been reported to have nearly uniform diameters between 30 and 50 nm with lengths varying from 500 nm to several micrometers [38], [39].

In this research, PANI nanofibers obtained by interfacial polymerization method were used in various formulations to obtain flexo printable compositions. These compositions were then used to print interdigitated targets using the rotary letterpress printing.

Results and Discussion

Due to the proprietary nature of commercially available silver filled inks, their exact composition was unknown. This posed difficulties in any attempts to modify their properties to suit given testing conditions. In order to have better control over properties, organic compositions based on polyaniline (PANI) nanofibers were formulated. Morphology of the products is largely affected by solvents and additives used. DBSA was used as a dopant and plasticizer in this work to effect ordered assembly of the PANI nanofibers in solutions with suitable surface tension characteristics.

PANI Nanofibers:

PANI nanofibers were synthesized in accordance with a procedure published by J. Huang and R. B. Kaner [38]. The formation of the nanofibers is illustrated in **Figure 27**. **Figure 28** shows the SEM images of the nanofibers.

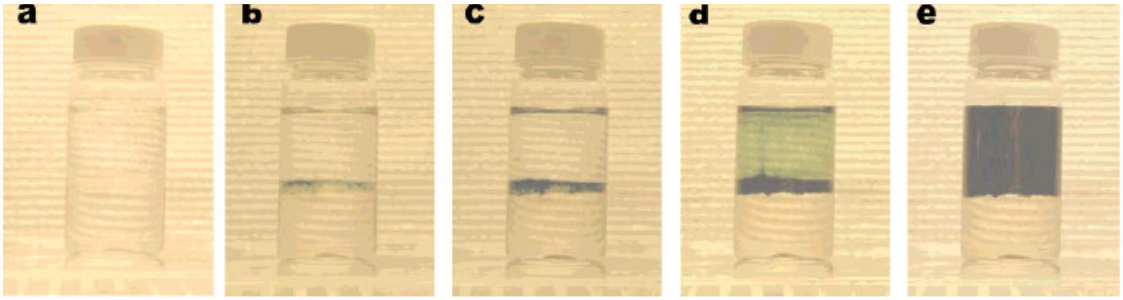

Figure 27: Interfacial Polymerization of Aniline in a Water/Chloroform System. (From a to e, the reaction times are 0, 1.5, 2.5, 4, and 10 min, respectively.) (J. Huang, et. al., J. AM. CHEM. SOC. 2004, 126, 851-855)

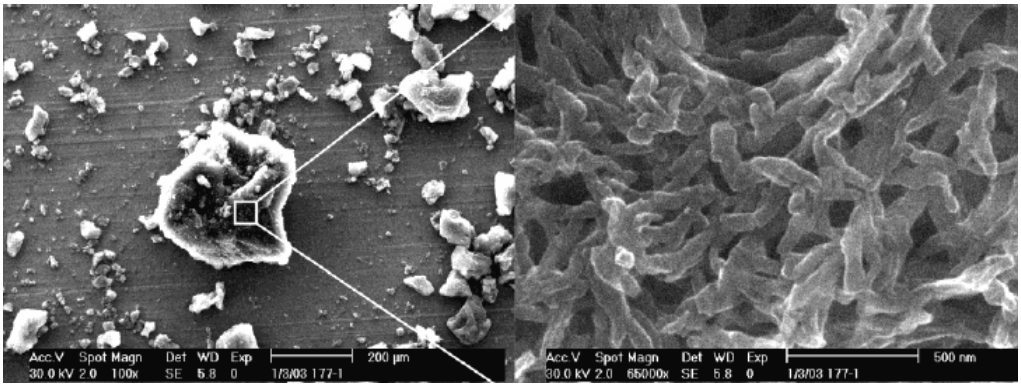

Figure 28: Polyaniline Powders Obtained after Filtration. Scanning electron microscopy images show that the powders (left; low magnification, ×100) are agglomerations of nanofibers (right; high magnification, ×65000) (J. Huang, et. al., J. AM. CHEM. SOC. 2004, 126, 851-855)

PANI Compositions:

The wet cake obtained after centrifugation of the PANI nanofiber was ~ 80 % solid by weight. This wet cake was used to formulate water based and solvent based printable compositions. In general the print quality decreased in the order xylene > mesitylene > toluene > water; with xylene showing the best results. Dodecyl benzene sulfonic acid (DBSA) can act as a dopant for PANI. However it is also known to act as a plasticizer when used in excess to give better PANI dispersions in organic solvents. In the formulations designed the DBSA content was varied between 1:0.5 to 1:2 weight ratio for PANI:DBSA. Good printable characteristic and conductivity was achieved with PANI : DBSA ratio 1:1 with xylene as solvent. **Table 6** summarizes the results based PANI-DBSA compositions.

	PANI : DBSA (weight ratio)	Moles of DBSA/mole PANI	Observed Composition Characteristics	Transfer Characteristics on Coated Paper Substrate
1	1:4	2.84	Viscous flow, cloggy fluid	Streaky non-uniform film layer
2	1:1.33	0.95	Viscous flowing fluid	Streaky broken film layer
3*	**1:1**	**0.71**	**Smooth flow, uniform fluid**	**Good transfer, uniform film**
4	1.0.5	0.34	Non-uniform fluid	Difficulty in transfer, non-uniform film
5	1:0	-	Dispersed fluid	Dispersed material, non-uniform film

Table 6: Observations for PANI-DBSA composition. *Best results.

Figure 29 illustrates the effect of DBSA content on printability of the compositions. It can be clearly seen that an optimum window of 1:1 weight ratio (for the given system of PANI nanofibers in xylene) exhibits the best printability. Addition of DBSA higher than 1 gm/gm PANI showed streaky patterns and non uniform thickness of the printed film. Addition of lower than 1gm/gm PANI showed difficulty in transfer of the compositions from the inking unit to the printing plate.

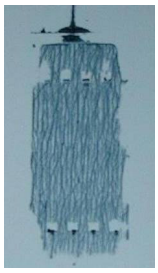

1:2 PANI:DBSA

3:4 PANI: DBSA

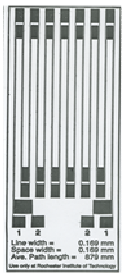

1:1 PANI:DBSA

1: (below) 1 PANI:DBSA

No DBSA (water based)

Figure 29: Print Quality for Varying Weight ratios of PANI:DBSA.

Hence it can be said that the amount of DBSA present in the system, influences the surface tension of the system and this parameter seems to be optimized at a weight ratio of 1:1. This composition contains a slight excess of DBSA than the molar amount required (~0.5 moles/mole EB) to obtain a conductive PANI salt. Hence it can be inferred that DBSA content below that required for protonation does not contribute towards plasticizing the mixture. A small excess of DBSA present in the system helps plasticize the system to give suitable printability. Any further increase in DBSA content deteriorates printability.

Printing on Flexible substrates:

The PANI ink also showed a good printability on plastic substrates. The printed film however showed better adhesion properties on paper than on the plastic substrate. The films printed at 0.2 m/s printing speed and 50 N printing force were found to have the best print quality for the PANI inks. **Figure 31** shows a test pattern printed on a flexible transparent PET film using the flexo process with the PANI ink.

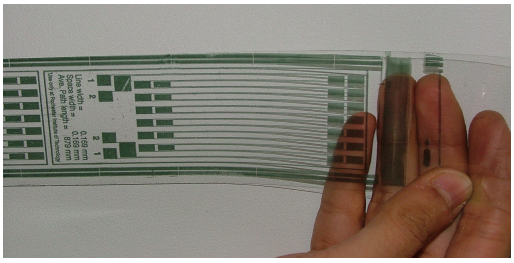

Figure 31: PANI ink printed of flexible PET substrate

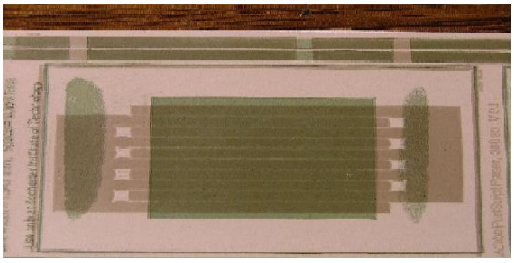

Figure 31: The all printed PANI gas sensor printed on the rotary letter press.

Successful Application: All printed gas sensor:

Error! Reference source not found. shows a PANI gas sensor that was designed and made entirely by printing. The sensor is a double layered structure with a layer of printed silver interdigitated electrodes and a PANI sensing layer on top of it. Due to the large difference between the sheet resistivities of the silver layer and the PANI layer, the performance of the sensor is not affected by the silver layer. The sensor was responsive to various gas vapors and gases and showed no hysteresis losses [40].

Summary and Conclusions

In the present study, emeraldine PANI nanofibrils were synthesized by interfacial polymerization. Various compositions were formulated from the nanofibers obtained. These compositions were tested for flexo printing at optimized printing parameters.

It was found that use of DBSA as in small excess as a dopant and plasticizer for the systems helps attain suitable surface energies to obtain printability. The optimized composition contained a 1:1 weight ratio of PANI:DBSA and showed a sheet resistance of ~1MΩ/□. The amount of DBSA used in the organic systems was found to have a direct effect on the printability of the compositions. This work shows a novel approach towards obtaining PANI-DBSA complex based flexo ink precursors.

An all-printed chemical vapor sensor was successfully fabricated by printing a PANI layer on silver interdigitated electrodes using flexographic printing.

The ink showed better adhesion on coated paper substrate than on flexible plastic substrates. However these inks demonstrated poor adhesion/rub resistance properties.

On the whole however, though organic functional materials are suitable for general use and short range applications as low cost alternatives, studies have proven that for higher performance applications lower resistance materials like metals are needed [41]. The performance of existing intrinsically conducting polymer (ICPs) devices is currently inadequate for operation as RFID tag at the frequency of choice, i.e., 13.56 MHz [42]. Due the high resistivity, even the PANI inks formulated could not be considered for antenna applications.

Experimental

PANI Synthesis:

The polyaniline nanofibers were synthesized by the procedure of J. Huang and R. B. Kaner [38], [39]. All chemicals were of analytical grade and used as received. A solution of aniline (3.2 mmol) in an organic solvent (chloroform) (10 mL) and another solution of ammonium persulfate (0.8 mmol) in 1M HCl as doping acid (10 mL) was prepared and mixed. Reaction was carried out at room temperature and allowed to run overnight. A characteristic green color of PANI emeraldine salt became visible indicating beginning of the polymerization reaction soon after the 2 phases came in contact. The product was purified by repeated centrifuging cycles using distilled water until the suspension reached a pH value of approximately 6. This product was then used for the formulations.

Ink Formulations:

Various different ink formulations were prepared with PANI nanofibers as conductive filler in a surface active organic matrix at 10% by weight of PANI in solution. Formulations with varying amounts of DBSA and various solvents were prepared at 50^0C with continuous stirring for 30 minutes. These were tested for printability. Sodium dodecyl sulphate (SDS) was tried in certain formulations as a surfactant and polyethylene oxide and polyacrylic acid were tried in certain formulations as viscosity modifying agents but no significant utility was found. Optimum properties were obtained from a formulation containing Dodecyl benzene sulphonic acid (DBSA) as a plasticizer to provide the required flow properties and xylene was used as solvent. Table 7 outlines the recipes for the printable formulations.

Table 7: PANI-DBSA Formulations

	PANI : DBSA (weight ratio)	Solvent (10% weight solution)
1	1:4	Xylene
2	1:1.33	Xylene
3	1:1	Xylene
4	1.0.5	Xylene
5	1:0	Water

Part C: Template polymerization of Thiophene in Micellar PS-b-PEO and PS-b-PAA Block Copolymers Systems.

Introduction

A new protocol for the preparation of a new semi-conductive/conductive dispersion based on polythiophene was explored. The following section highlights the work done in this regard.

Poly (thiophene-2, 5-diyl) (PT) and its derivatives are perhaps the most extensively studied class of conducting polymers. This class includes linear PT and PT mono-substituted at the 3 position or at the 3 and 4 positions [43]. PT is often considered as a model conductive polymer to study charge transport in polymers with a nondegenerate ground state due to its representative nature with regard to polaron/bipolaron interactions [28], [43]. Polythiophenes exhibit good conductivity [44], and high stability to oxygen and moisture [45] compared to most other intrinsically conductive polymers. Studies also have shown that they have a range of useful characteristics such as solubility and processibility [46], ease of synthesis [45], stereoregularity in certain cases [47]. **Figure 32** shows the structure of poly (thiophene-2, 5-diyl).

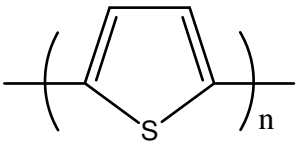

Polythiophene

Figure 32: Poly (thiophene-2, 5-diyl): (PT)

In the present work, two strategies for the templated polymerization of thiophene were developed. The first is the templated polymerization of PT in a micellar or vesicular block copolymer system catalyzed by an oxidative coupling reagent using which the thiophene was sequestered or bound. The second is a variant of this system in which the block copolymer micelles are swollen.

One of the most significant barriers to the use of a high molecular weight thiophene-2, 5-diyl polymer is that does not contain substituents at the 3- or 3, 4- positions making it insoluble. Smith et al.,[48], [49] have reported that block copolymers of polystyrene (PS) and poly(ethylene oxide) (PEO) and that of PS and poly(acrylic acid) (PAA) complexed with metal salts form vesicular/micellar structures in solution and thereby provide specific micro-domains in the solution, which can be utilized as reaction sites for

localized template guided polymerization of thiophene. The PT thus obtained is not in itself soluble, however, since it is localized within the core of the micellar or vesicular block copolymer, nanostructured aggregate or ensemble is soluble. Transparent films can be cast from these solutions. In block copolymer systems having PEO or PAA content greater that 25% by volume, the morphology of films cast from micellar or vesicular solutions can be induced to be cylindrical (worm-like), or lamellar and somewhat bicontinuous, depending on how the spent catalyst, Fe^{2+} is removed and the composition the solvent system. The resistance of these films can thus vary significantly, depending on the morphology of the final product.

Results and Discussion

Templating PT using a micellar or vesicular block copolymer system:

In this research we sought to leverage the disclosures of Smith et al., to create "soluble" compositions containing high molecular weight PT that could be formulated to yield semiconductive, film-forming inks. This section details the results of our studies on the use of a block copolymer for template polymerization of thiophene and the degree to which a bicontinuous, semiconductive composition suitable for formulation of an ink with suitable characteristics for printing can be obtained.

Template polymerization involves the polymerization of a monomer in the presence of a pre-formed polymer or other materials. The repeat residues in the pre-formed template are typically different from that of the monomer being polymerized [50]. In this type of polymerization, the monomer or polymerizing entity is generally associated with or bound to the macromolecule being used as the template. The association (physisorption or chemisorption) may be the result of covalent bonds, ionic bonds, hydrogen bonds, ion dipole forces or Van Der Waals interactions. The template generally interacts with the monomer to predispose a multiplicity of monomer units toward polymerization. The template polymerization process may thus give precise structures and microstructures that are complementary to that of the template [51].

The literature [52], [53] teaches that it is possible to use amphiphilic copolymers as templates for preparation of complex nanostructures. In recent years, there has been a considerable progress in the use of block copolymers as templates for the controlled synthesis of nanoparticles and mesoporous inorganic materials. The self assembly of the copolymers has been used to engineer a variety of templates of different sizes and topologies [54]. Improvements in the mechanical properties and stability of the conducting polymers have been reported using template polymerization. Templating also influences the morphology of the end product [55]. Homopolymers and random copolymers have generally been used as templates to polymerize the conductive entity to form the conductive composites [48], [55].

Block copolymers are known to form various crystal-like nanomorphologies on a length scale between few nanometers to several hundred nanometers [54]. Copolymer morphologies that have been observed are: spherical (S), cylindrical (C), lamellar (L), and bicontinuous including perforated layers (PL) and gyroid (G) structures. Different nanoscale morphologies can be obtained in diblock and triblock copolymer systems by changing the volume fraction of the respective phases and solvents [56]. A sketch illustrating these structures is shown in **Figure 33**

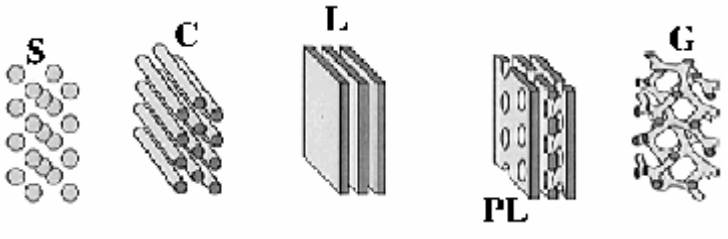

Figure 33: Copolymer Morphologies
(http://www.chem.ufl.edu/~reu/main/projects/lecommandoux.htm)

2,2-Bithiophene (BT) was used as the material to be templated for this study because it has a lower oxidation potential than thiophene and can be polymerized chemically with oxidizing agents as mild as $FeCl_3$.

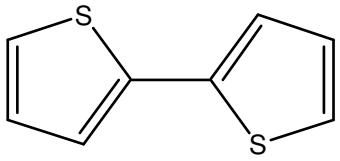

2,2-bithiophene

Figure 34: 2,2-Bithiophene

Ferric chloride ($FeCl_3$) was used as the oxidative coupling agent and catalyst. The ferric ion can be dissolved in poly(ethylene oxide) and poly(acrylic acid) with Fe^{3+} typically being solvated in hexacoordinated sites by ion-dipole forces between the metal ion and non-bonding electron pairs on oxygen atoms of oxyethylene or carboxylic acid residues in poly(ethylene oxide) and poly(acrylic acid), respectively.

Schematic structures of the metal polymer complex that may thus be formed are depicted in **Figure 35** (a) and (b).

a)

b)

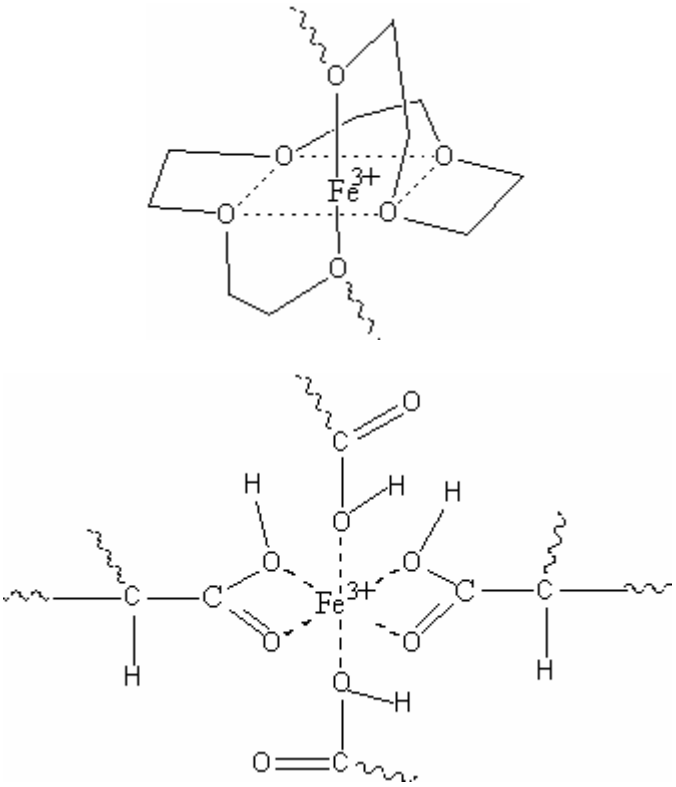

Figure 35: a) Fe^{+3} complex with oxygens from the PEO segment. b) Fe^{+3} complex with oxygens from the PAA segment.

Polystyrene-block-polyethylene oxide (PS-b-PEO) and polystyrene-block-polyacrylicacid (PS-b-PAA) were used as matrices. It was reported elsewhere that these copolymers form vesicular and micelle structures in solution when complexed with metal salts [48], [49], [57]. In toluene solutions, addition of ferric ion leads to the formation a micelle or vesicle with a solvent phobic core containing the complexed ferric ion that will be the catalyst for the oxidative coupling of BT. The micelles serve as tiny reaction sites for polymerization of the monomer that diffuses in to the micelle core. The micelle core effectively sequesters all of the $FeCl_3$ introduced into the system. The BT monomer introduced into the system, thus, is expected to polymerize only in the cores of the micelles.

The templated polymerization of thiophene in Fe^{3+}-doped micellar or vesicular block copolymer solutions was initially carried out using a mixture of toluene and

dimethoxyethane (DME). The polymerization, however, did not go well in this solvent mixture. In order to determine the effect of the presence of DME on the oxidative coupling of BT, the templated polymerization was carried out in toluene, without added DME. In the absence of DME, the oxidative coupling of BT proceeded rapidly.

Figure 36 illustrates the reaction process through the polymerization of BT in the micellar or vesicular polymer solution.

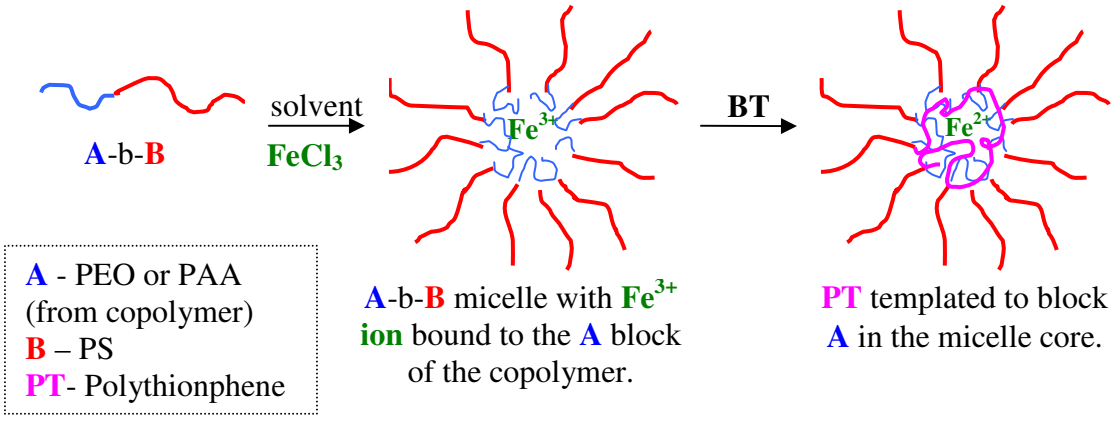

Figure 36: Schematic of Micellar Copolymer Template Polymerization

The templated conducting polymer so obtained can subsequently be precipitated and washed with a solvent capable of extracting Fe^{2+} from the system. Theoretically, a solvent can be chosen so as to generate films that retain a spherical micellar structure or "invert the core" and yield cylindrical, lamellar or bicontinuous morphologies. The morphologies obtained are in principle, determine by the nature of the solvent system, the volume fraction of POE or PAA, the amount of PT generated in the templated polymerization and the conditions under which the film is cast, dried and annealed. The advantage of this process is that the end product is obtained as a solution in a solvent that can be directly used in an ink formulation.

In this work, hexane was used as the initial precipitation solvent. The hexane precipitate was then extracted with a mixture of hexane and methanol so as to prevent inversion of the polymer micelles and emulsification of the composition. The extracted composition was then redispersed (redissolved) in toluene, xylene, ethylaactetate and tetrahydrofuran.

Swelling of Copolymer Micelle with Homopolymer in Templating PT:

Within the core of block copolymer micelles, there is a "free volume". Accordingly, micelles in such a system can be swollen by adding a homopolymer common to the segment of the copolymer that forms the core. In order to be incorporated in the block copolymer core, the molecular weight of the added homopolymer must be less than that of the corresponding block copolymer chain segment that forms the core. The degree to which the block copolymer core can be swollen is about 30% [58]. This fact provides a convenient option for increasing in the volume fraction of oxyethylene or carboxylic acid chain segments within the core of micellar solutions of PS-b-POE for PS-b-PAA, respectively. The amount of PT that can be generated within the core of a copolymer micelle is determined by the amount of Fe^{3+} that can be bound in the core and that quantity is in turn directly proportional to the volume fraction of oxyethylene or carboxylic acid chain segments.

This option was exploited to swell PS-b-POE micelles by 30% with low molar mass POE. The core of the swollen micelle was subsequently doped with a greater amount of $FeCl_3$ which in turn enabled the incorporation of more PT with each swollen micelle. **Figure 37** shows a schematic cartoon of the swelling of the micelle core and the formation of PT within this swollen micelle core.

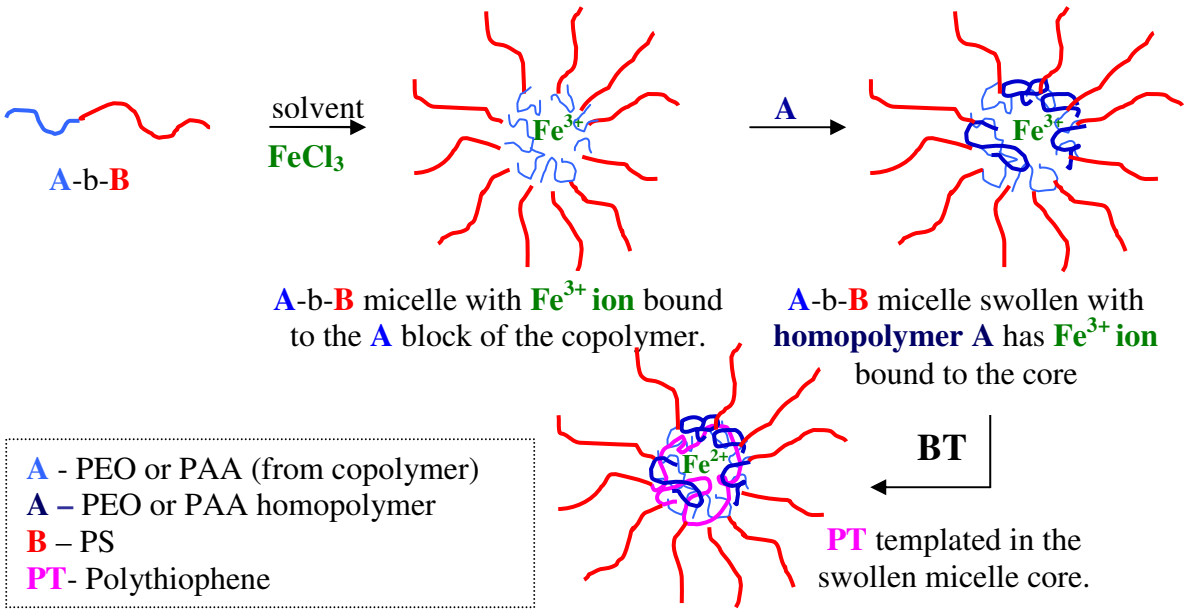

Figure 37: Schematic of a Swollen Micelle Reaction System.

In this process, the molecular weight of the homopolymer employed in the swelling of the copolymer micelles was varied. When PS-b-POE micelles were swollen with poly(oxyethylene) having a number average molecular weight (Mn) of only 750 g/mole, PT was lost during the process of removing Fe^{2+} from the system. One might speculate that the molecular weight of PT templated in the presence of the 750 g/mole POE homopolymer was correspondingly low in molecular weight. When a POE homopolymer with a higher Mn (5000 g/mole) was used to swell the PS-b-POE micelles PT was retained in the system after removal of Fe^{2+}.

The POE swollen reaction mixtures were precipitated in hexane and a mixture of hexane and methanol was used to extract the Fe^{2+}. It was observed that the reaction product phase separated into 2 phases if the methanol content was higher than the hexane content in the extraction solution. The Fe^{2+} from the product was hence extracted through a series of hexane methanol washes keeping a higher hexane content in order to avoid phase separation and emulsification of product.

A flow chart outlining the processes of templated polymerization of BT in micellar or vesicular block copolymer solutions and the templated polymerization of BT in

homopolymer-swollen micellar or vesicular block copolymer solutions is shown in **Figure 38.**

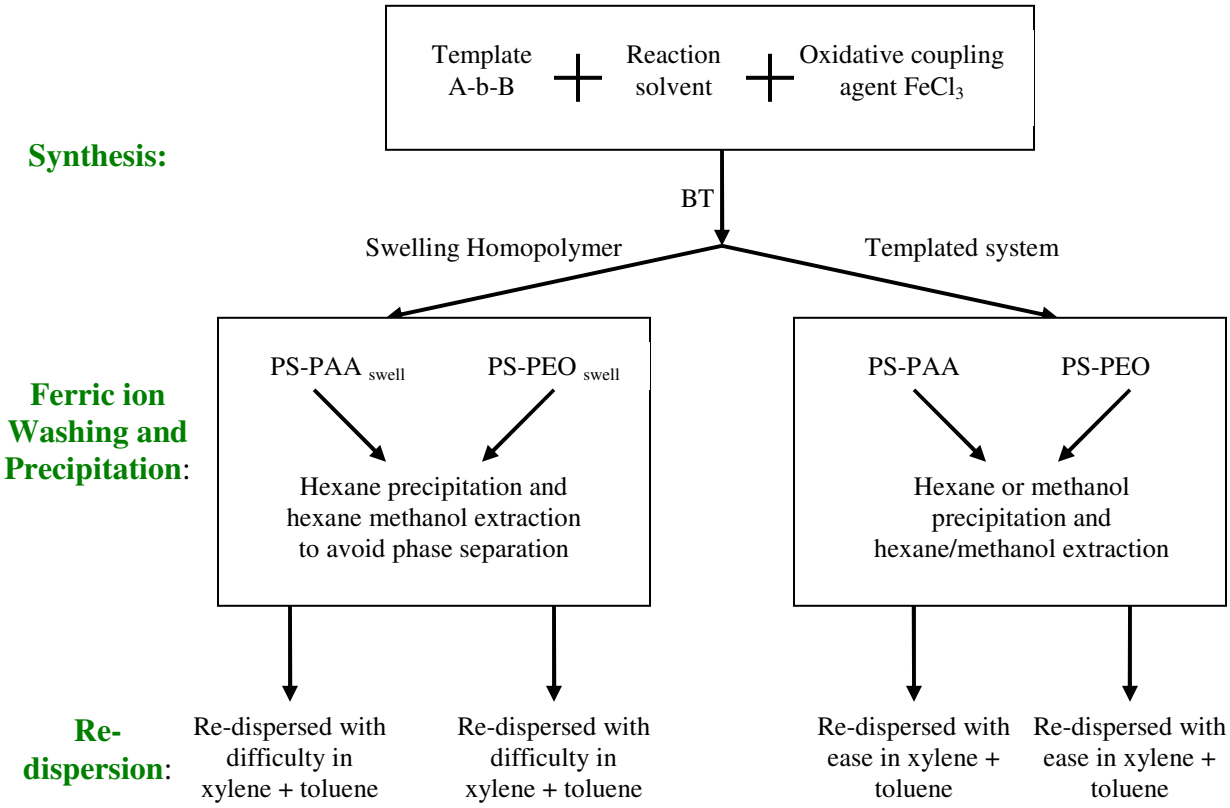

Figure 38: Flow process for polymer synthesis and ink formulation

The experimental section provides detailed recipes and procedures for the templated polymerization of BT in Fe^{3+} micelles of PS/POE and PS/PAA and POE swollen PS/POE copolymers.

IR analysis:

Figure 39 shows FTIR spectra for PT composites obtained using PS-b-PEO as the template. One might expect the peaks observed in the spectra to be representative of a mixture of PS, PEO and PT. This is indeed the case. The literature cites the peaks that may be specifically attributed to PT. These include 3060, 1490, 1440, 1350, 1070, 900, 830, 785 and 695 cm^{-1}. in the composite spectra show in **Figure 39** only the peak ~753 cm^{-1} has no interference from peaks in the PS-b-PEO copolymer.

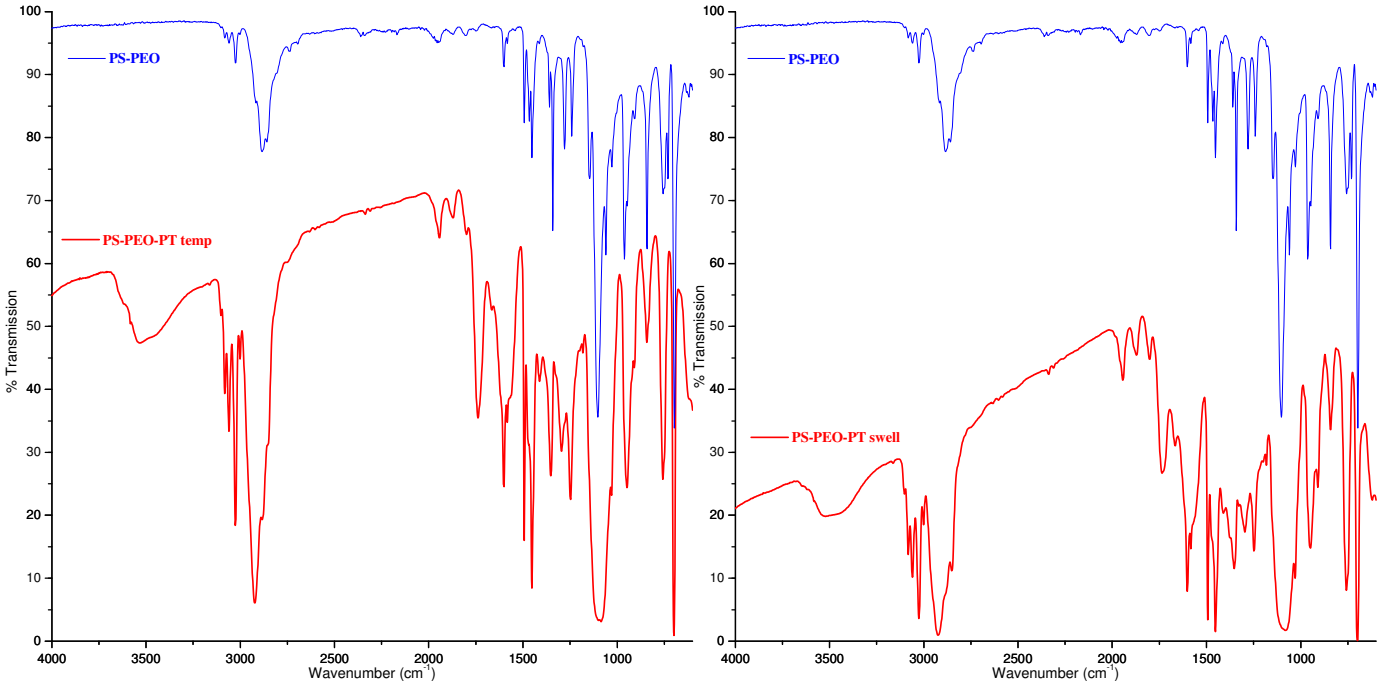

Figure 39: FTIR spectra for a) PS-b-PEO Templated PT and b) PS-b-PEO Swell-Templated PT.

Table 8 [59], [60] gives approximate peak assignments for the polymer system under consideration.

Table 8: General IR signature for PS-b-PEO block copolymer

General peak assignments for block copolymer PS-b-PEO	
900-690 (cm^{-1})	out of plane bends in aromatics
1300-1000 (cm^{-1})	C-O-C stretching bands for ethylene oxide
1450, 1375 (cm^{-1})	C-H bend
3000-2850 (cm^{-1})	C-H stretch

Figure 40 shows spectra wherein an attempt was made to subtract the spectrum of PS-b-PEO from that of the compositions to give the spectrum of PT. The subtraction does not eliminate all copolymer peaks but makes enhances the PT peaks.

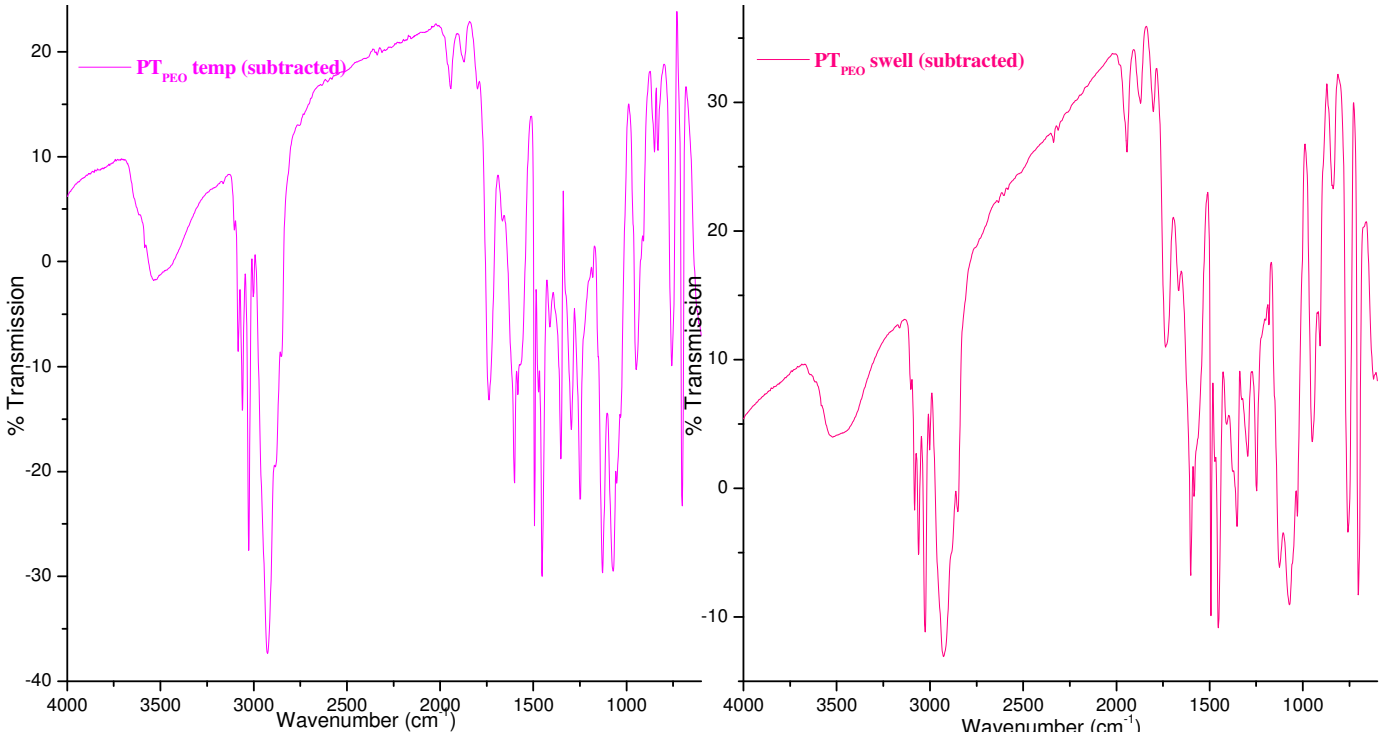

Figure 40: FTIR Subtracted Spectra for PS-PEO systems.

In a study conducted by G. Louarn et. al., spectral signatures for PT have been modeled using oligothiophenes [61]. A detailed study of the present system based on the model used has been highlighted below indicating dominant signature peaks can be found in the present subtracted PT spectra.

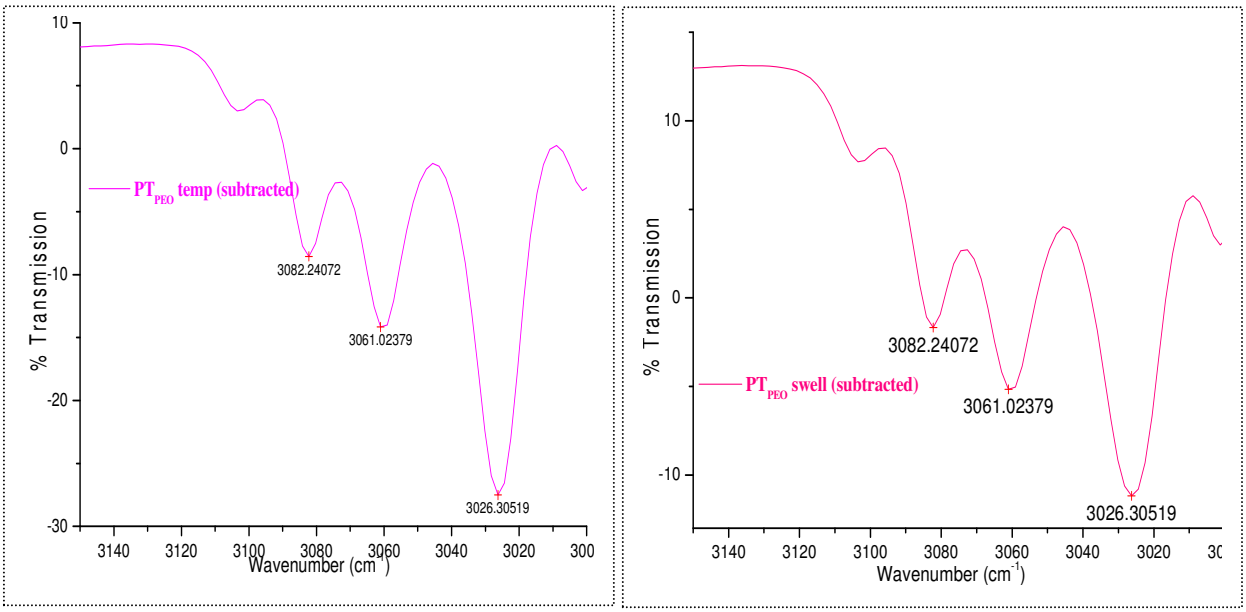

Figure 41: IR Region 3200 to 3000 cm^{-1}

Figure 41 shows strong double bands at 3061 and 3082 cm^{-1}. These can be assigned to (aromatic) C_β-H stretching vibrations. The splitting of bands indicates different conformations. This may be taken as an indication of crosslinking of the PT formed.

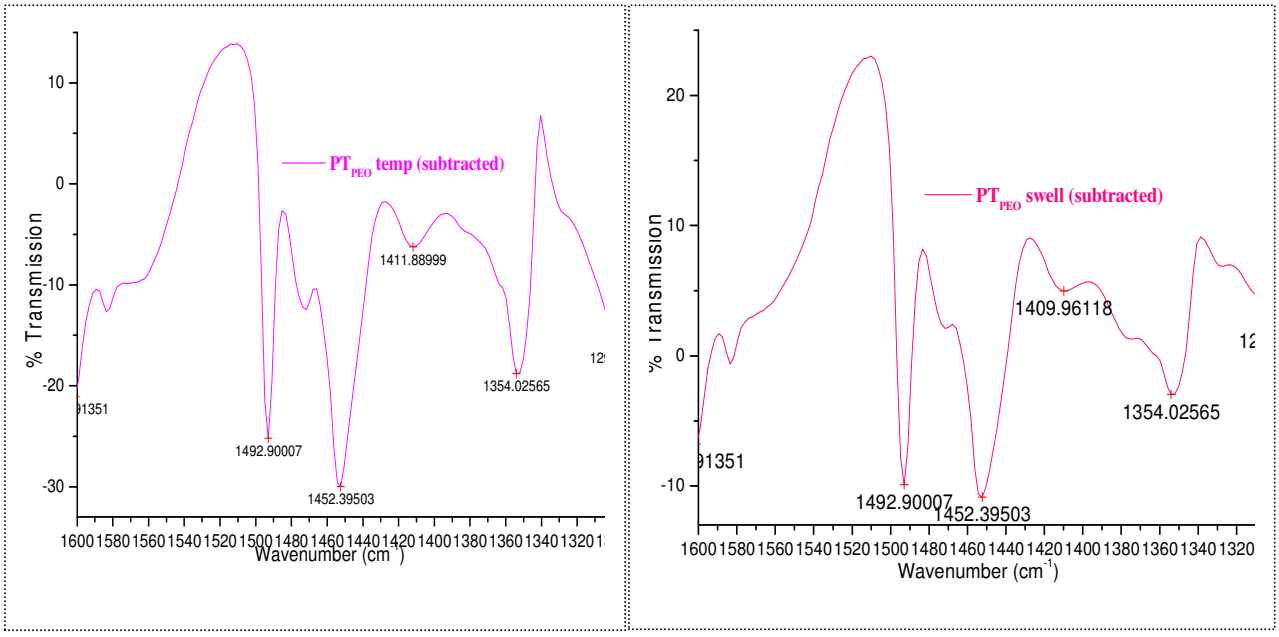

Figure 42: IR Region 1600 to 1300 cm-1

Figure 42 shows the region 1600 to 1300 cm^{-1}. The peak at 1354 cm^{-1} represents the C_β-C_β stretching vibration which is not affected by the chain length of PT formed. Region

around 1450 cm^{-1} indicates active C=C and C-C vibrations. 1492 and 1452 cm^{-1} are the dominant peaks.

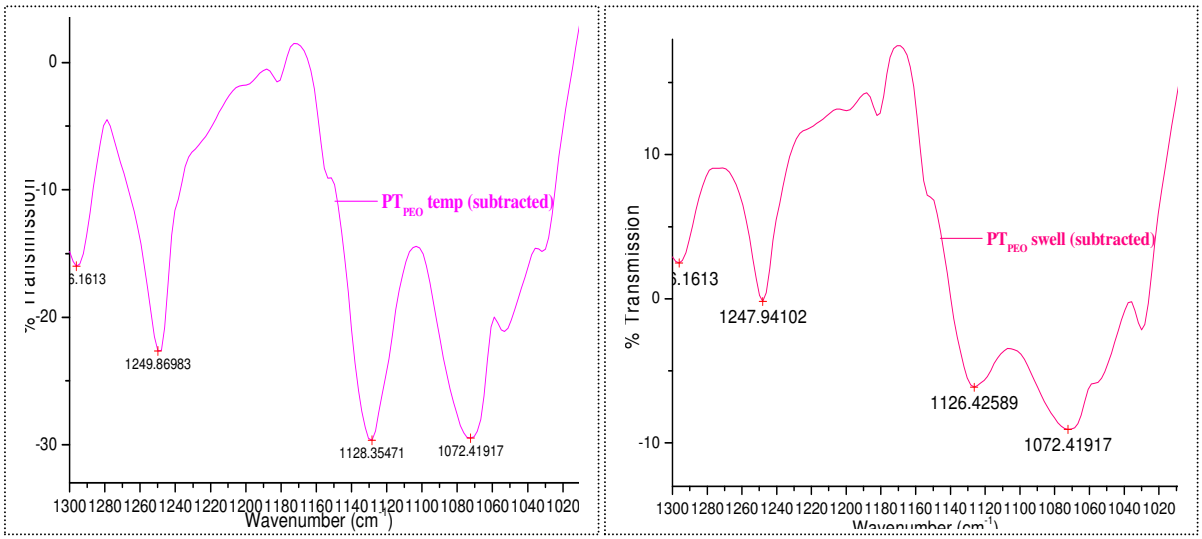

Figure 43: IR Region 1300 to 1000 cm^{-1}

Figure 43 shows the details in the region 1300 to 1000 cm^{-1}. The band at ~1240 is assigned to C-C inter-ring vibration and that at ~1070 to C_{β}-H bending vibration.

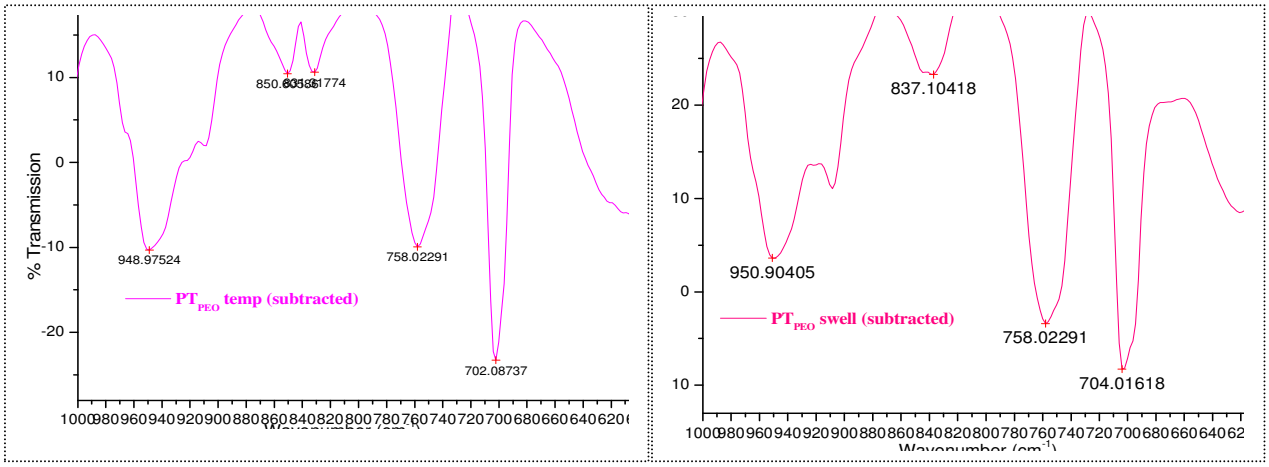

Figure 44: IR Region 1000 to 600 cm^{-1}

Figure 44 shows bands characteristic of the C-H out of plane deformations. Some of these bands are slightly off from those in the model. However this may taken as a nominal shift in the band positions due to the difference in chain lengths of the compounds studied in the model and that obtained in the present samples. The dominant bands here are ~830, ~760 and ~700 cm^{-1}

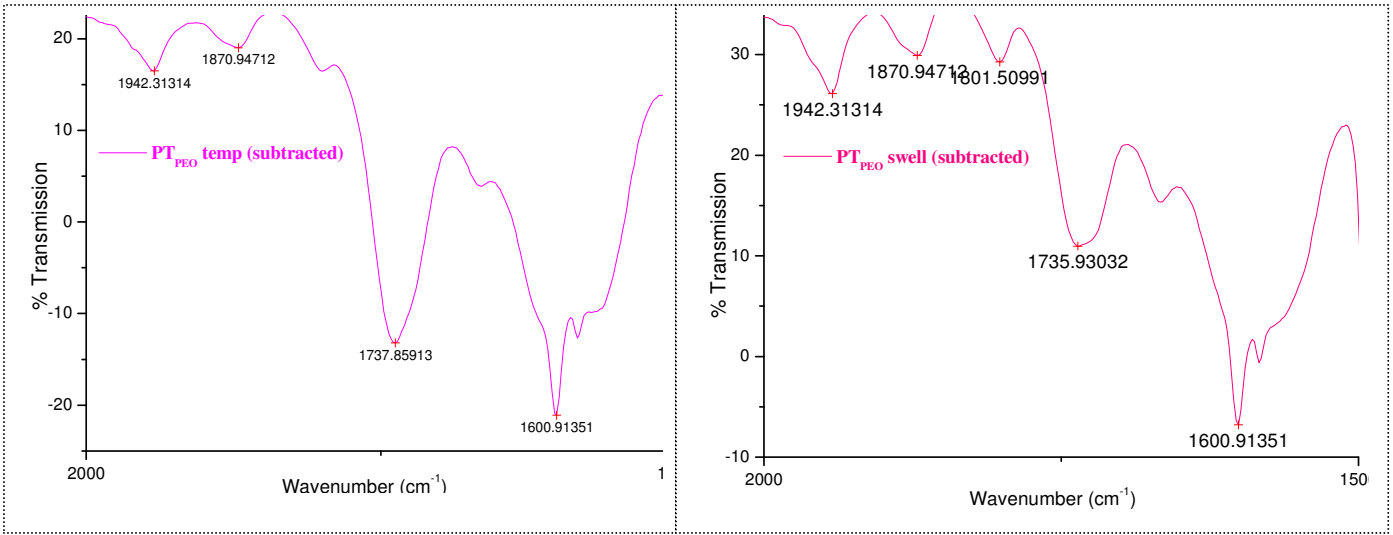

Figure 45: Anomalies in IR Spectra

Figure 45 shows the region 2000-1500 cm^{-1} that contains multiple peaks in the spectra for the composites that do not signify PT but are also absent in the base copolymer. The peaks can be assigned to vibrations of carbonyl group [62]. A study by Shenglong Wang et. al. [63] reports oxidative decay of PT forming a C=O group in the material due to degradation of the thiophene ring. In the present system, templating of PT using $FeCl_3$ and the binding catalyst in PS-PEO block copolymer shows an apparent oxidative degradation leading to formation of the C=O and O-H groups. The peaks respective to these froups can be seen in the region 2000-1500cm^{-1} and ~3500cm^{-1} respectively in the IR spectra for this system. The carbonyl and hydroxyl groups may form either due to oxidative degradation of PEO or PT

The IR results for the template polymerization of PT using PS-PAA have been discussed below. **Table 9** [62], [64] shows the general peak assignments for the PS-PAA matrix used in the present system.

Table 9: General IR signature for PS-b-PAA block copolymer

General peak assignments for block copolymer PS-b-PAA	
860-690 (cm^{-1})	Out of plane bends in aromatics/substituted benzene ring
1250-1200 zigzag (cm^{-1})	Stretching vibration of C-O
1448-1600 (cm^{-1})	C-C oscillation frequency of benzene ring
3000-2850 (cm^{-1})	C-H stretch in benzene ring

Figure 46 shows FTIR spectra for the PS-PAA system. One might expect the peaks observed in the spectra to be representative of a mixture of PS, PAA and PT.

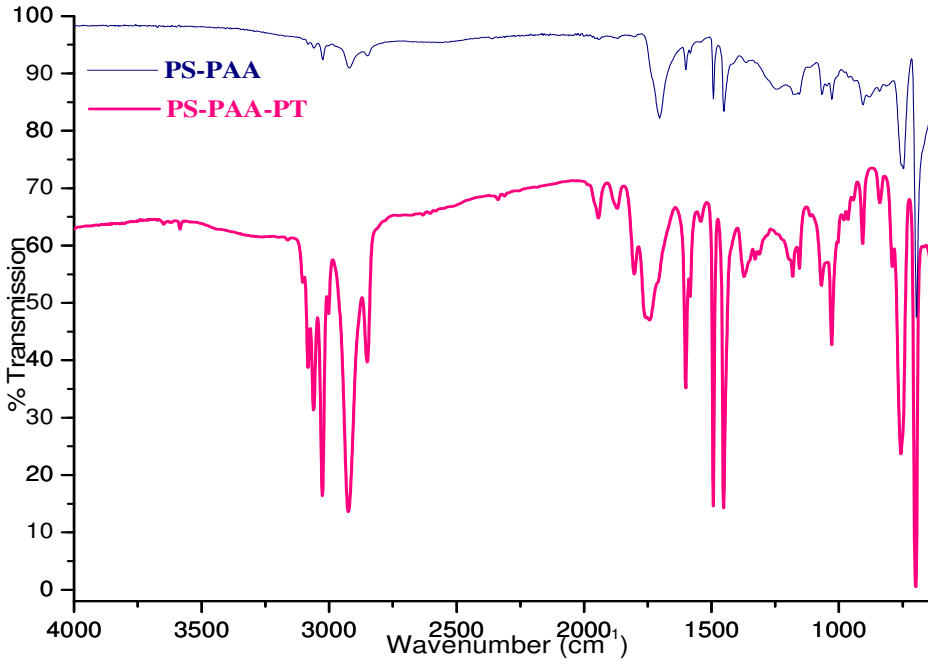

Figure 46: FTIR spectra for PS-b-PAA block copolymer and templated PT Composite.

In this case as well a detailed look at the subtracted spectrum of PT reveals signature PT peaks. **Figure 47** shows FTIR subtracted PT spectrum.

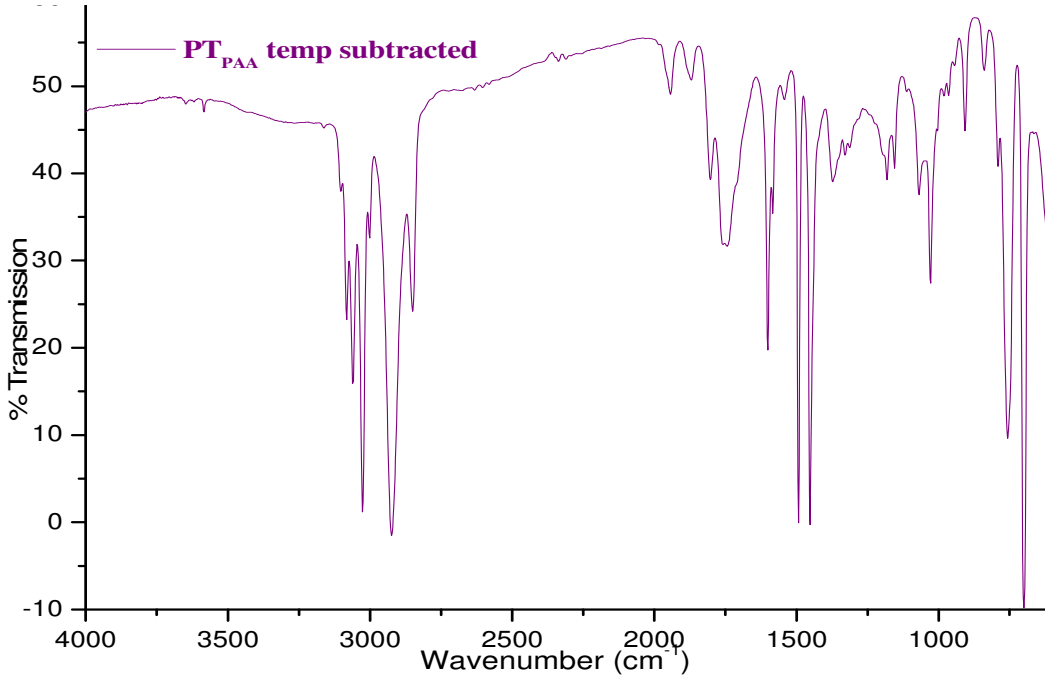

Figure 47: FTIR subtraction of copolymer PS-PAA from that of PT

Figure 48 shows the details of the PT subtracted spectrum from the PS-PAA composite. This spectrum too shows similar dominant peaks as those observed in the PEO subtracted spectra, for example, 3060, 1490, 1450, 1375, 1180, 1020, 900, 830, 750 and 700 cm^{-1}. The strong peaks observed in the range 860-690 and 3024 indicate presence of the thiophene ring in the system. A double peak is clearly observed at 3060 and 3026 cm^{-1} which can be assigned to C_β-H stretching vibrations based on the model. Again, presence of double peaks at many positions could be taken as an indication of crosslinking at various positions in the PT formed. Peaks are observed at 1452 and 1492 cm^{-1} consistent with data from the model. The peak at 1373 cm^{-1} can be assigned to the C_β-C_β stretching vibration. The peak near 1020 cm^{-1} can be assigned to C_β-H bending vibrations. Peaks observed at 700 and 900 cm^{-1} can be assigned to a substituted thiophene ring indicating crosslinking.

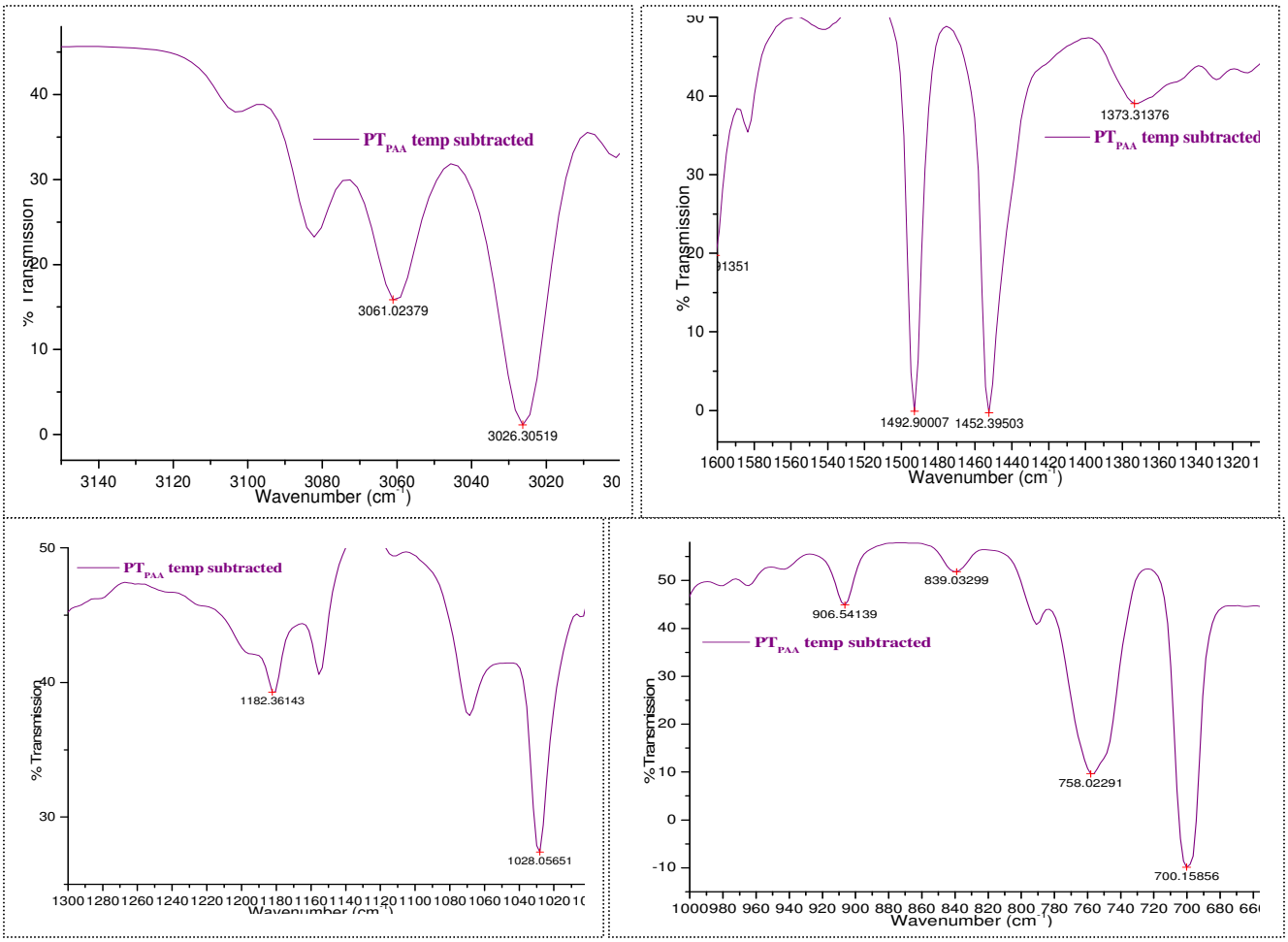

Figure 48: IR Details for the PS-PAA-PT Composite.

Bands present in the 2000-1500 cm^{-1} range are again characteristic of C=O group which in this case may belong to the templating copolymer since spectral subtraction does not eliminate those bands completely from the PT spectrum.

BT template polymerized in presence of PS-b-PAA does not appear to undergo oxidative degradation to any significant extent. The UV-vis results give a further insight into the degradation phenomenon of the PT in PEO systems and not in the PAA systems.

UV-vis analysis:

Figure 49 shows the UV-vis spectra for the PS-b-PEO template polymerization system. As can be seen from the figure, the block copolymer did not show any transitions beyond 300 nm. The undoped PS-PEO-PT composite exhibited a band edge 423 nm and an absorption maxima at 370 nm. Iodine doping of the sample broadened the peaks significantly and showed a significant shift in the peaks. This may be due to the absorbance picked up due to disproportionation of iodine to form I^{3-} and I^{+} ions in the system. Nitorsonium Hexafluoro Antimonate (NHFA) was also used as dopant. The UV-vis of the NHFA doped PT composite showed a definite broadening of peak and a shift in band edge to 462 nm.

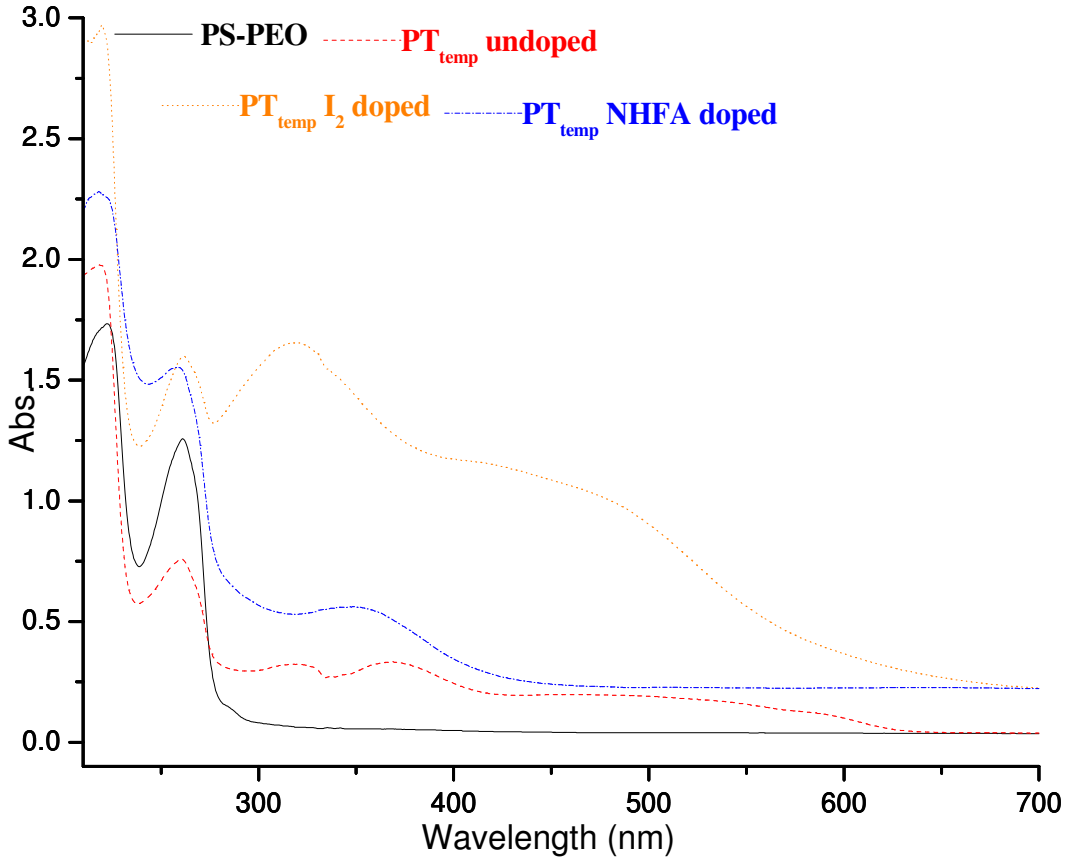

Figure 49: UV-vis spectra of a) PS-b-PEO b) Templated PT c) I2 doped templated PT d) NHFA doped templated PT

Figure 50 shows the UV-vis spectra for the template polymerization scheme carried out in presence of swollen PS-b-PEO micelles. In this case too the iodine doping seemed to show a peak broadening again picking up absorbance due to the iodine ions present in the system. The undoped polymer showed maxima at 363 nm with narrow peaks. The NHFA doped sample did not show a significant red shift but it did however exhibit considerable broadening of the peaks.

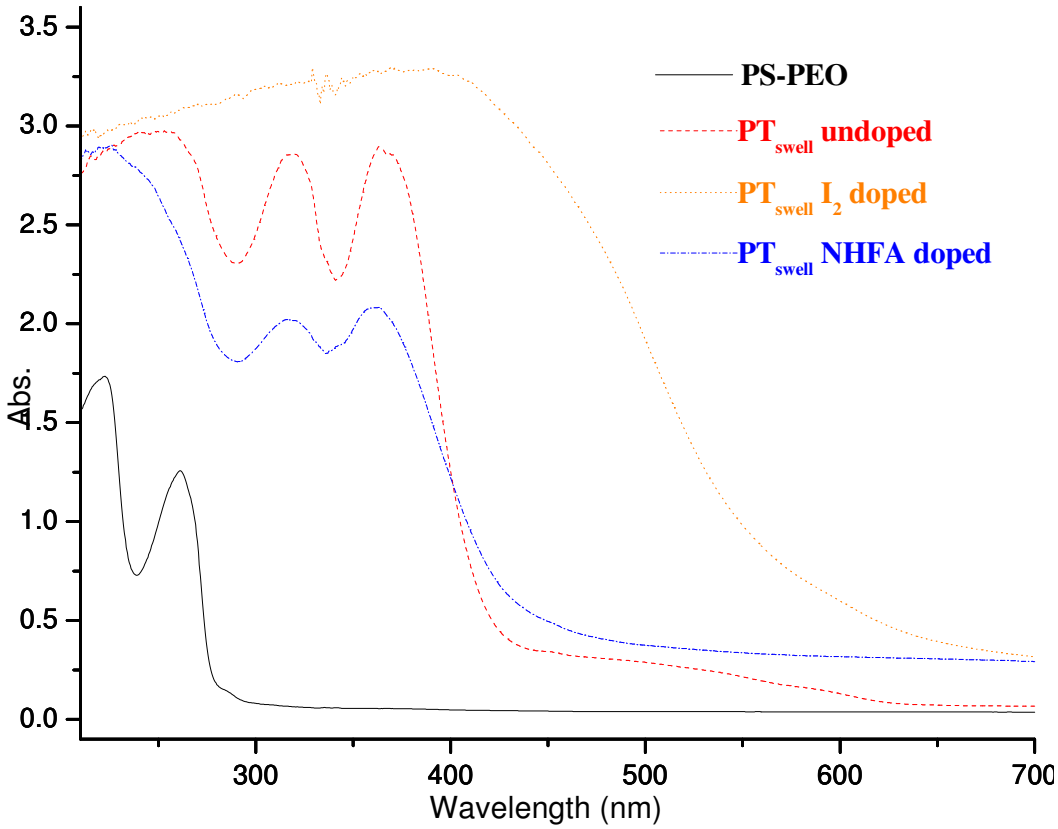

Figure 50: UV-vis spectra of a) PS-b-PEO b) Swollen micelle templated PT c) I2 doped swollen micelle templated PT d) NHFA doped swollen micelle templated PT

Figure 51 shows the UV-vis spectra for the template polymerized PT on PS-b-PAA copolymer. In this case, iodine doping did not show a change in color in the film. Hence a UV-vis spectrum was not obtained. A distinct color change from red to blue was observed in the NHFA doped sample solution. The undoped sample exhibited an absorption maxima at 499 nm. Doping of the sample led to a tremendous broadening of the peak and shift of the maxima into the near IR region.

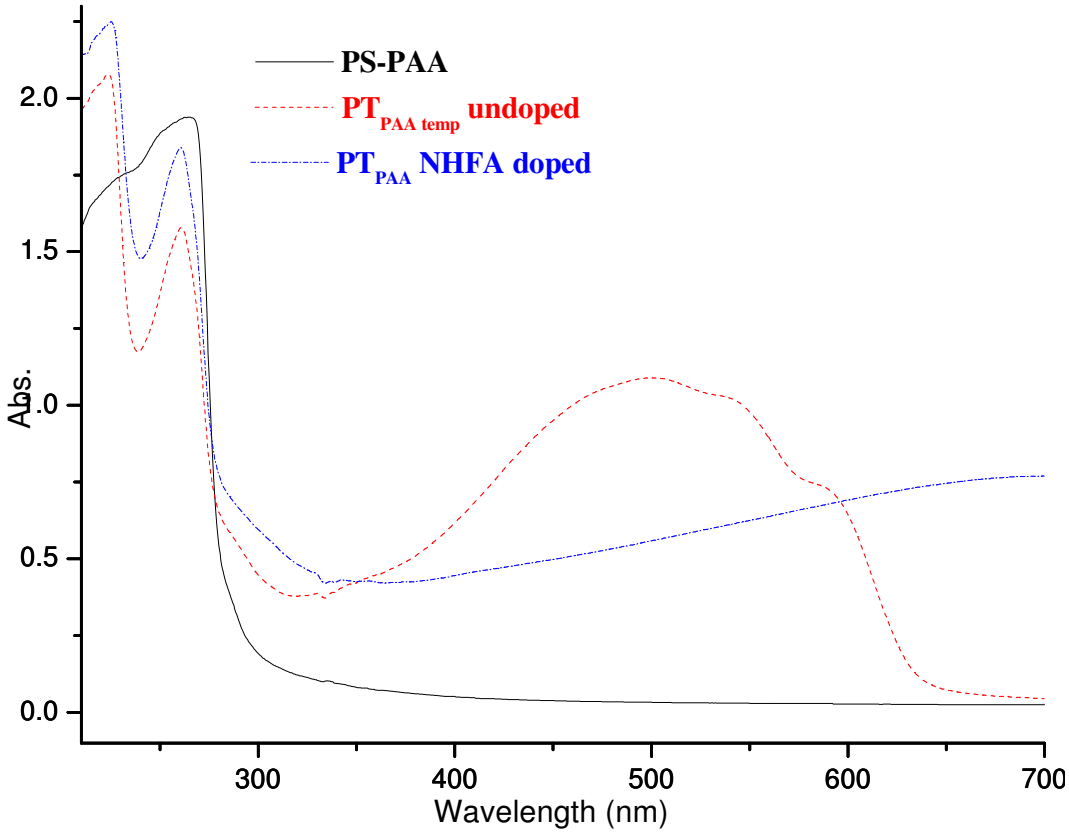

Figure 51: UV-vis spectra of a) PS-b-PAA b) Undoped Templated PT c) NHFA doped templated PT

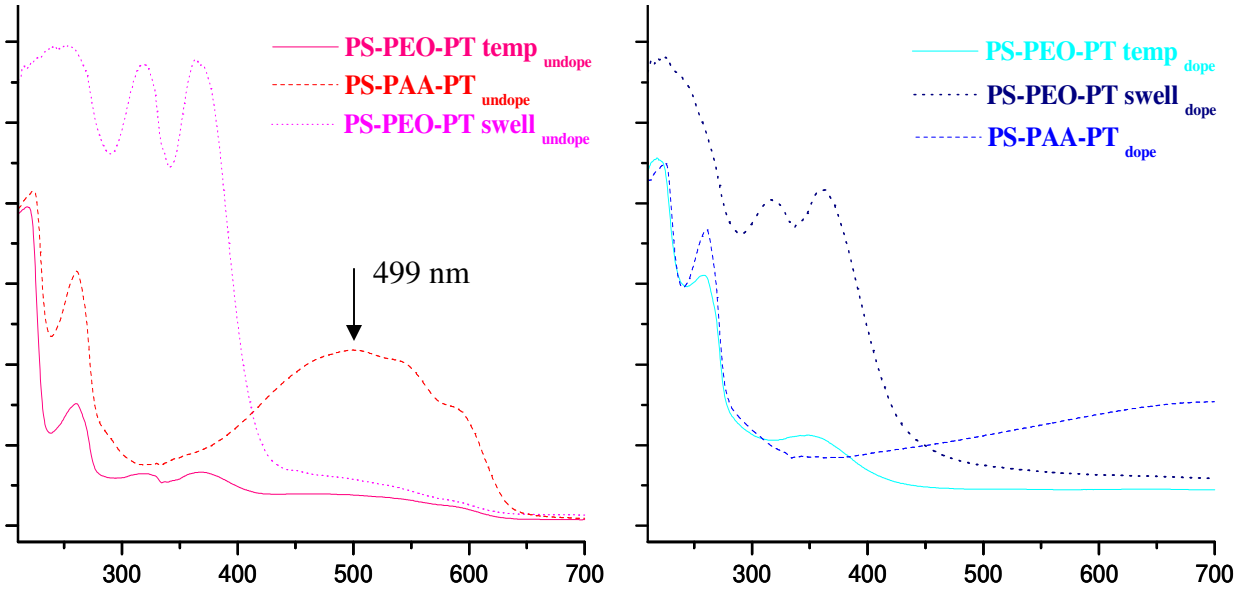

Figure 52: UV-vis Spectra of Undoped and Doped Comparable Systems

Figure 52 shows UV-vis spectra for undoped and doped PT composites of PS-PEO and PS-PAA. The difference in the UV-vis absorbance of PT in the two systems in both the doped and undoped states is apparent from the spectra. This difference may indicate an apparent solvatocromic effect of PT in the two phases PEO and PAA. Solvatochromic effects have been reported in the case of many substituted PT.

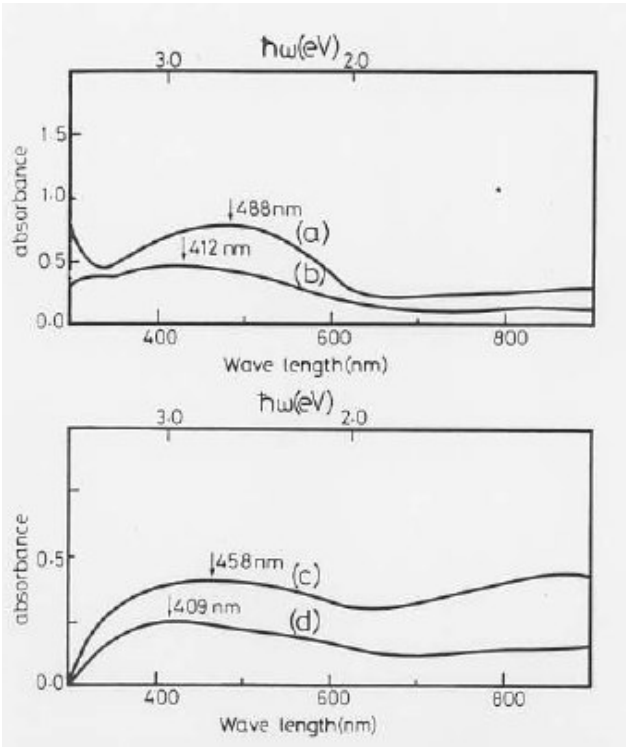

Figure 53: UV-vis Absorption Spectra of a) Undoped PT, b) Undoped Degraded PT, c) Doped PT and d) Doped Degraded PT [63]

However an important phenomenon may be considered based on the results obtained. **Figure 53** shows UV-vis spectra from degradation studies of PT [63]. The figure indicates pronounced maxima for non-degraded PT at 488 nm and a slight bulge in the range 600-400 nm

for degraded PT. The UV-vis of the PS-PAA-PT system shows pronounced maxima at 499 nm similar to that observed in non degraded PT. The PS-PEO-PT composites exhibit the slight bulge similar to that observed in the degraded PT sample in the range 600-400 nm. The spectra for the doped materials too show a similar trend, as observed in case of degrading of PT.

Hence it can be inferred based on the IR and UV-vis results that PS-PAA is perhaps a more stable system for templating PT without leading to oxidative degradation of PT.

DSC analysis:

Figure 54 a) shows a complete DSC cycle for the PS-b-PEO copolymer. As is clear from figure b), the copolymer exhibits a strong crystallization peak characteristic of the PEO segment. The Tg of PS appears at 100°C apparently lower than that of the literature value of PS homopolymer (104°C)

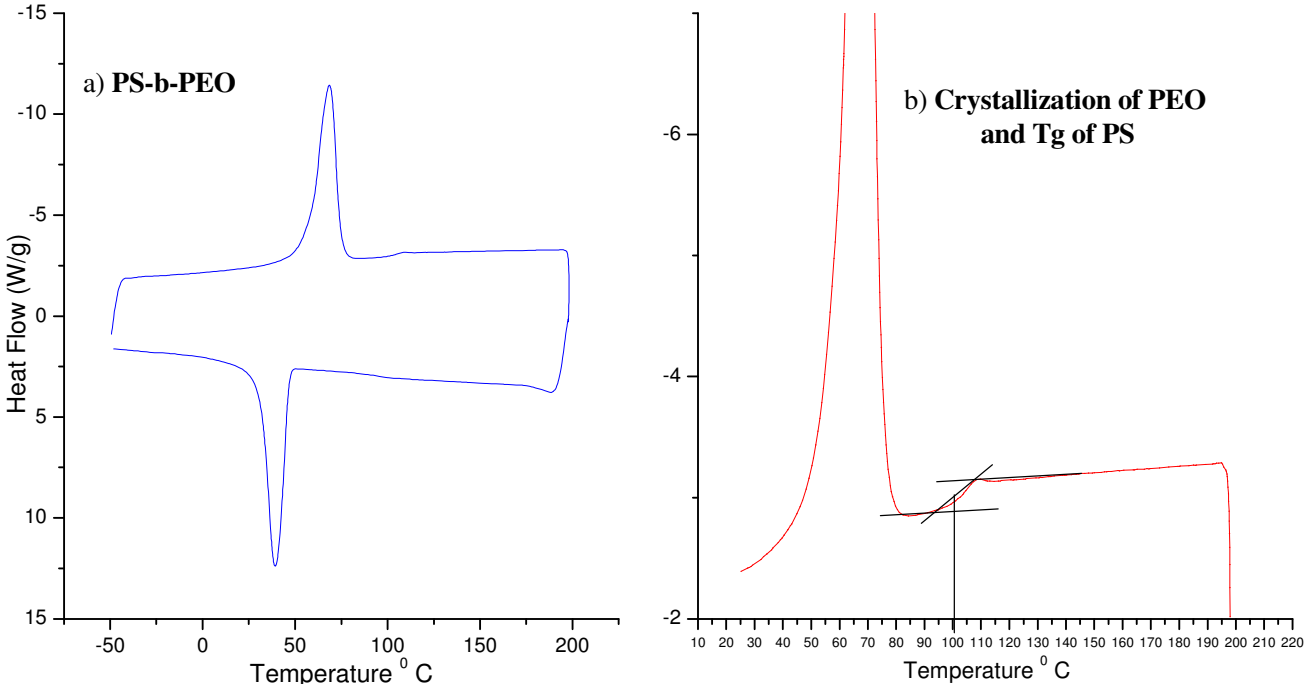

Figure 54: a) Complete DSC cycle for PS-b-PEO b) Crystallization peak for PEO and Tg for PS

The PT present in the PS-PEO systems affects the thermal transitions of the copolymer. This can be seen in the DSC curves of the PS-PEO system in **Figure 55.** The figure shows a part of the 2nd cooling cycle for the pure copolymer, the template PT composite and the swollen-micelle template composite. The crystallization peak of PEO is apparent in the copolymer DSC curve. This curve also indicates a glass transition at ~ 104°C characteristic of the PS segment. The crystallization peak disappears in the templated sample curve and the Tg transition shows a shift to a lower temperature. With an increase in the PT content (in the swollen-micelle sample curve), the crystallization peak is completely suppressed and Tg transition for PS shows a further shift to a lower temperature. Disappearance of the PEO crystallization peak indicates a strong association

between the templating segment and the polymer formed. The decrease in the Tg transition for PS indicates that some amount of mixing in the phases has taken place and that the PT may be present in the PS phase as well as the PEO phase of the copolymer.

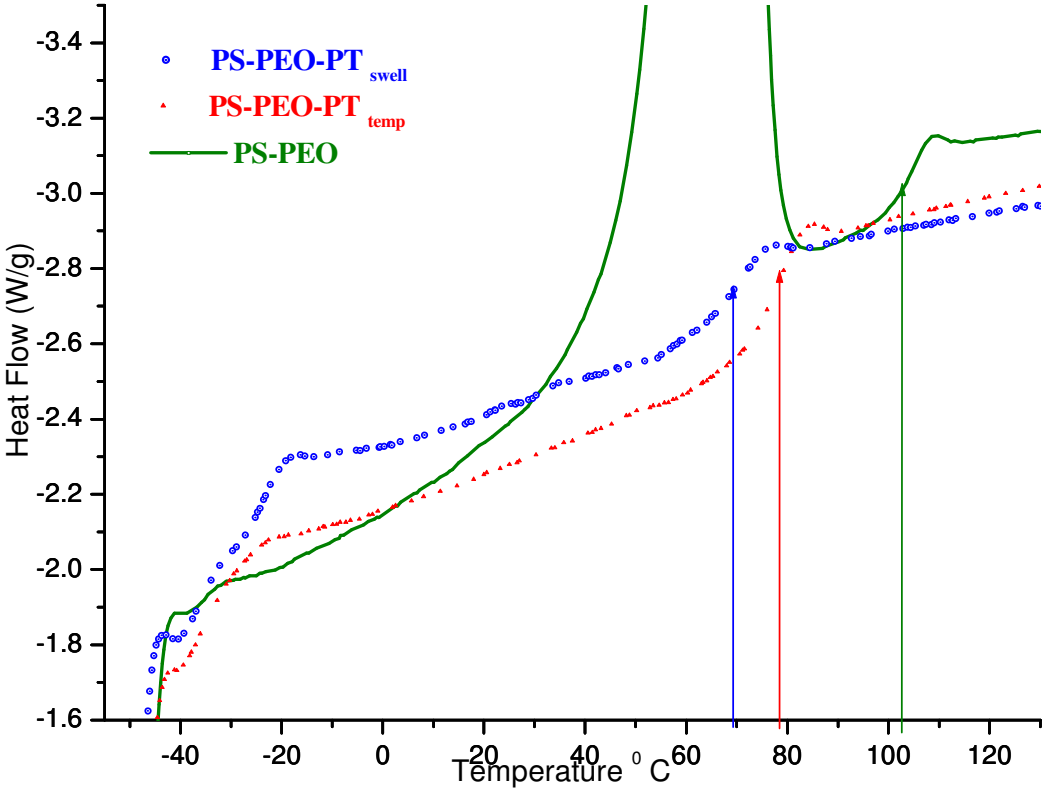

Figure 55: DSC curves showing the effect of PT content on the thermal transitions of PS-b-PEO

Changes induced in the thermal transitions of PS-b-PAA due to presence of PT in the system have been depicted in the DSC curves shown in **Figure 56**. The figure shows a cooling cycle of the copolymer PS-b-PAA (blue solid curve) clearly indicating two glass transition temperatures at 104°C (dotted blue line) corresponding to that of PS and the other at 121°C (solid blue line) corresponding to that of the PAA phase in the copolymer. The cooling curve for PS-PAA-PT (orange triangle embedded curve) shows a clear suppression of the Tg corresponding to the PAA phase and a single Tg (dotted orange line) lower than that of PS in the copolymer, at 89°C. Thus it can be concluded that in this system as well the PT is not only closely associated with the PAA phase on which it was templated but is also present in the PS phase.

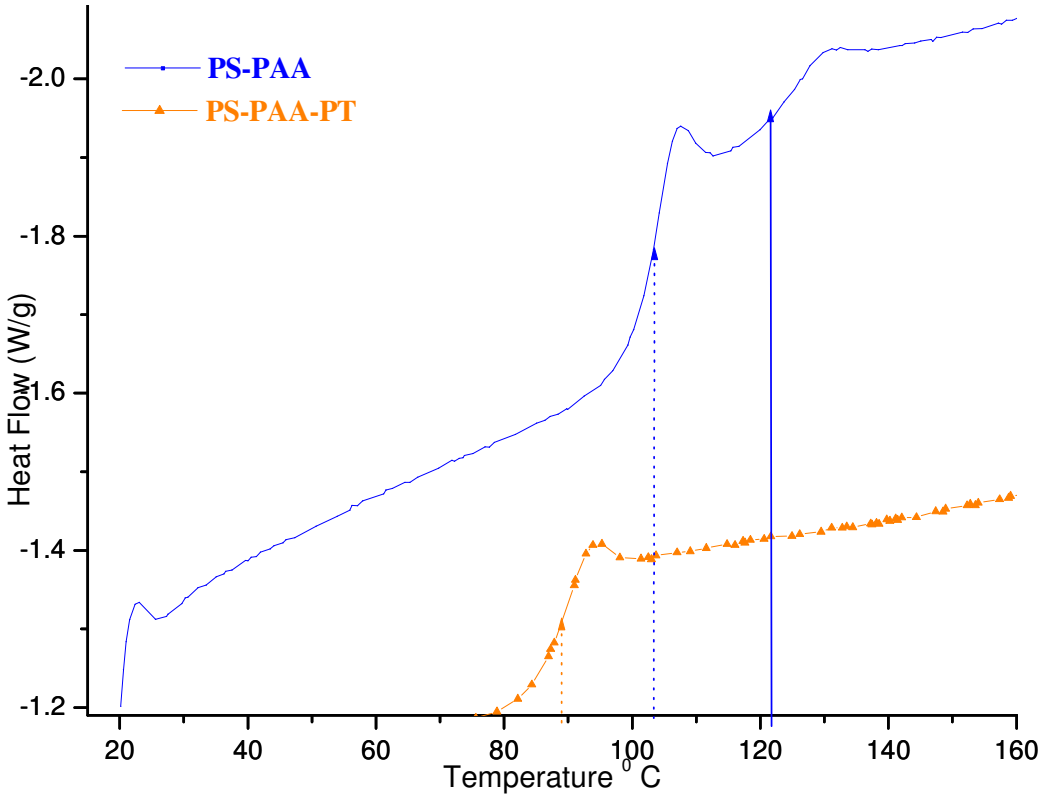

Figure 56: DSC curves showing the effect of PT content on the thermal transitions of PS-b-PAA

Summary and Conclusions

A novel approach has been demonstrated for the 1st time to obtain re-dispersible PT systems using template polymerization. Template polymerization of BT was carried out in vesicular/micellar reactor systems comprising of amphiphilic copolymer systems with an oxidative coupling agent ($FeCl_3$) bound onto the amphiphilic segment. This approach was attempted in order to obtain a redispersible PT system. The three systems studied in this research were:

1) Template polymerization of BT in PS-b-PEO.
2) Template polymerization of BT in PS-b-PEO swollen with PEO homopolymer.
3) Template polymerization of BT in a PS-b-PAA matrix.

The end products could be easily re-dispersed any of a wide variety of solvents for the PS segment of the block copolymer, ie. toluene, xylene, tetrahydrofuran, ethyl acetate. Compositions re-dispersions in tetrahydrofuran or ethyl acetate showed better film forming characteristics. The PS-PEO/PT composite systems re-dispersed more readily than did the PS-PAA/PT composites.

FTIR and UV-vis analysis revealed some interesting results. The nature of the amphiphilic segment in which the template polymerization occurred, was a key factor in the oxidation stability of the PT formed therein. An apparent oxidative degradation of the PT was observed when template polymerization was carried out in the PS-PEO matrix using $FeCl_3$ as the binding catalyst. The degradation was also apparent in the UV-vis spectra of the PS-PEO/PT composites. After purification and removal of the ferric and ferrous ions, employed in the polymerization, the composite products obtained were doped/oxidized NHFA. Doped films cast on NESA glass substrates showed no significant conductivity. This lack of conductivity is likely the result of an inability to invert the micellar morphology due to crosslinking of the PT in the core. It may also be due to insufficient volume fractions of conducting phase in the template polymerized systems. In case of PS-PEO/PT, degradation of the PT could be attributed to loss of conductivity. Therefore, we cannot rule out the possibility of an insufficient volume fraction of the

conducting phase or the oxidative degradation of the conductive polymer as factors in leading to loss in conductivity.

DSC results on the final products gave unequivocal evidence that the PT was sequestered principally in the domains of the amphiphilic polymer segment. However, the glass transition temperature of the PS phase was also perturbed.

Experimental

Materials

All chemicals were used as received. The source and quality of materials used is as stated below.

Reactants used:
The block copolymers PS-b-POE and PS-b-PAA were obtained from the archive of Thomas W. Smith. These polymers were synthesized by sequential living anionic polymerization process, the reference of which can be found in the US patent 6,605,236 (Smith et. al.) [49]

Details:
PS-b-POE (NB# 23407-96-3): 66.2 mol% POE block copolymer - molecular weight 58K -b-48.1K. (PS segment has a molecular weight of 58,000 g/mole and the POE segment has a molecular weight of 48,100 g/mole)
PS-b-POE (NB# 23407-6): 21.72 mol% POE block copolymer – molecular weight 75.9K-b-8.9K (molecular weight of the PS segment is 75,900 g/mole and that of POE is 8,900 g/mole.
PS-b-PAA (NB# 25567-27 hydrolyzed): The composition of the block copolymer is 80.6 mol % styrene, 18.8 mol% acrylic acid, 0.1% t-butylacrylate, 0.4 mol % methylacrylate.

2,2-Bithiophene, (97%), (Aldrich); Iodine (Aldrich); Ferric chloride, (98%), (Aldrich); Nitrosonium Hexafluoro Antimonate, (NHFA), (99.9%), (Aldrich); Homopolymer Poly(ethylene glycol) methyl ether, (PEO), (Aldrich)

Solvents used:
Toluene, (99%), (Acros Organics); Dimethoxyethane, (DME), (99%), (TCI America); Methanol, (99.9%), (J. T. Baker); Nitromethane, (Mallinckrodt Baker Inc.); Hexane, (100%), (J. T. Baker); Tetrahydrofuran, (THF), (100%), (J. T. Baker); Ethyl acetate, (99.5%), (Mallinckrodt Chemicals); Xylene, (Acros Organics)

Copolymer Templating of PT

Synthesis of PS-b-PAA/PT composites in xylene

2 g of PS-b-PAA (80.6 mole % PS) was dissolved in a xylene. 0.83 M solution of $FeCl_3$ in nitromethane was added to the solution keeping the acrylic acid to ferric ion ratio at 3:1. 2,2-bithiophene was added to this reaction system (at 60^0C) keeping the ferric ion to BT ratio 2.69:1. The reaction product instantly turned blue on addition of the BT monomer. This product was then washed and precipitated using methanol to remove the residual ferric ions. The washed product was then re-dispersed in xylene to obtain the ink.

Synthesis of PS-b-PEO/PT composites xylene

2 g of PS-b-PEO (66.25 mole % PEO) was dissolved in a xylene. 0.98 M solution of $FeCl_3$ in nitromethane was added to the solution keeping the ethylene oxide to ferric ion ratio at 5:1. 2,2-bithiophene was added to this reaction system (at room temperature) keeping the ferric ion to BT ratio 2.69:1. The reaction product gradually turned blue-green on addition of the monomer. Since this product contained a relatively larger amount of the PEO segment, it was difficult to precipitate and wash it using methanol. The product was hence precipitated using hexane and washed using a mixture of methanol and hexane. The product was then re-dispersed using toluene as solvent for the ink formulation.

Synthesis of PS-b-PEO/PEO 5000/PT composites in xylene

2 g of PS-b-PEO (66.25 mole % PEO) was dissolved in a xylenes. PEO homopolymer (Mn: 5000) equivalent to $1/3^{rd}$ the number of moles of PEO present in the copolymer were added to swell the copolymer micelles in solution. 0.98 M solution of $FeCl_3$ in nitromethane was added to the solution keeping the total ethylene oxide to ferric ion ratio at 5:1. 2,2-bithiophene was added to this reaction system (at room temperature) keeping the ferric ion to BT ratio 2.69:1. The reaction product turned blue on addition of the monomer. Since this product contained a relatively larger amount of the PEO segment, it was difficult to precipitate and wash it using methanol. The product was hence precipitated using hexane and washed using a mixture of methanol and hexane. The product was then re-dispersed using toluene as solvent for the ink formulation.

Comparative synthesis of PS-b-PEO/PT composites in toluene and toluene/DME

2 g of PS-b-PEO (82.3 mole % PS) was dissolved in the reaction solvent. 0.83 M solution of $FeCl_3$ in nitromethane was added to the solution keeping the oxyethylene to ferric ion ratio at 5:1. 2,2-bithiophene was added to this reaction system (at room temperature) keeping the ferric ion to BT ratio 2.69:1. When the reaction solvent was DME-toluene (1:4 volume ratio) the characteristic blue color that accompanies the Fe^{3+}-catalyzed polymerization of bithophene was not observed. It was washed and precipitated in methanol to remove the ferric ions. The product was a light pink polymer that did not did not re-disperse in toluene. With toluene as the reaction solvent however, the reaction mixture rapidly turned blue on addition of bithiophene. The reaction product was washed and precipitated in methanol to remove the ferric ions. The final product was a dark pink colored flaky material that did not re-disperse in toluene.

Synthesis of PS-b-PEO/PEO/PT composites in toluene/DME (to study effect of swelling homopolymer molecular weight)

A total of 2 gm of PS-b-PEO (82.3 mole % PS) and homopolymer PEO with a weight ratio of 90% total PEO was used. This was dissolved in a mixture of DME-toluene (1:4 volume ratio). The solution thus obtained consisted of swollen copolymer micelles and an excess of dissolved homopolymer. 0.83 M solution of $FeCl_3$ in nitromethane was added to the solution keeping the total ethylene oxide to ferric ion ratio at 5:1. 2,2-bithiophene was added to this reaction system (at room temperature) keeping the ferric ion to BT ratio 2.69:1. This reaction was carried out in 2 sets, one with the swelling homopolymer PEO of number average molecular weight (Mn) of 750g/mole and the other with Mn of 5000 g/mole. The reaction product did not give the characteristic blue color obtained on polymerization of BT. The resultant products were precipitated in hexane in order to avoid the micelle core inversion. The ferrous ions were removed in a soxhlet extraction apparatus by dialysis of the precipitate, contained in a cellophane dialysis tube, against methanol. When the block copolymer was swollen with PEO 5000 the reaction product retained in the 2000 molecular weight cut off dialysis tube was a red particulate solid (presumably PT) mixed with a white precipitate (presumably a mixture of PS-b-PEO and

PEO) The red precipitate could not be redispersed in toluene. When the block copolymer was swollen with PEO 750 the reaction product was a white precipitate that was soluble in toluene.

Doping

Two methods were used for doping.

a) Free standing films of the samples were exposed to iodine vapor till an obvious color change was observed.
b) The sample solutions were doped using NHFA as the doping agent. A 1:3 molar ratio was kept for BT: NHFA for maintaining the maximum doping level.

Resistance Measurements

Films were cast of the solutions on NESA glass substrates and resistance was measured across a 5 mm gap using the digital multimeter model M810B from CE.

Infrared Spectroscopy

This technique was used to verify the structure of the synthesized polymers based on the peaks obtained. A Bio-Rad Excalibur Series FTS 3000 instrument was used to analyze the various samples using a diffuse reflectance cell. Two sets of samples were prepared. In one set free standing films cast from the sample solutions of the material were used to obtain IR spectra and in the other set films were cast on NaCl pellets from the sample solutions and dried at 165^{o}C to ensure complete removal of moisture from the systems. The spectra were obtained from 4000-600 cm^{-1} and 32 scans were obtained for each sample. The resolution was set at 1 cm^{-1}.

Ultra violet Spectroscopy

Ultraviolet spectroscopy was used to examine the shift in the band edges due to doping of samples. Absorbance spectra in the range 210-700 nm were obtained for the purpose of the study. A Shimadzu 2501PC UV-Vis Spectrophotometer was used. The slit width was 5 nm. Sample films were cast on quartz plates.

Differential Scanning Calorimetry

Presence of PT in the system was identified using the phase transitions observed in the DSC scans for the pure copolymers and the composites. TA Instrument 2010 DSC was used to carry out the analysis. The sample weight was kept in a range of 5-10 mg.

References

[1] http://www.ece.gatech.edu/research/labs/vc/theory/photolith.html

[2] Robert F. Service, *Patterning Electronics on the Cheap,* Science, 278, 17 Oct, (1997)

[3] David Harrison, Blue John Ramsey, Peter Sidney Albert Evans, US Patent # 6,356,234

[4] Edward C, *PEDs are Coming, Printable Electronics and Displays,* Printed Electronics 2004, Dec 7 (2004), New Orleans. USA

[5] Ramsey B.J.; Evans P. S. A.; Harrison D.; *A Novel Circuit Fabrication Technique Using Offset Lithography*, Journal of Electronics Manufacturing, 7, 63, (1997)

[6] Seppo Pienimaa, Risto Ronkka, *Towards Printed Products,* Printed Electronics Europe 2005, Cambridge, UK, April 19-20 (2005)

[7] Tommi Remonen, *Organic Electronics: From Basic Research to Production,* Printed Electronics, 14-15 September 2004

[8] P. Calvert; *Inkjet Printing for Materials and Devices*, Chem. Mater, 13, (2001), p. 3299

[9] Burns, et. al., *Inkjet Printing of Functional Materials -Inkjet Printing of Polymer Thin-Film Transistor Circuits*, MRS Bull., 28(11), Nov 2003.

[10] Sangoi, R.; Smith, C.G.; Seymour, M.D.; Venkataraman, J. N.; Clark, D.M.; Kleper, M.L.; Kahn, B.E.; *Printing Radio Frequency* Identification (RFID) Tag Antennas using Inks Containing Metal Nanoparticles, J. of Dispersion and Science Technology, (2004), 25 (4), p. 513.

[11] Lochun D.; Kilitziraki M.; *Post-processing of Conductive Lithographic Films for Multilayer Device Fabrication*, IEEE/CPMT Int'l Electronics Manufacturing Technology Symposium, (1999)

[12] Harrey P. M.; Ramsey B.J.; etc.; Capacitative Type Humidity Sensor Fabricated Using the Offset Lithography Printing Process, Sensor and Actuators B, 87, (2002), p. 226

[13] Shepherd, P. R.; Evans, P. S. A.; Ramsey, B. J.; Harrison, D. J.; *Lithographic Technology for Microwave Integrated Circuits*, Electronics Letters, 33 (6), (1997), p. 483

[14] Evans, P S A; Harrey, P M; Ramsey, B J; Harrison, D J; *Integrated Circuits - RF Circulator Structures Via Offset Lithography*, Electronics Letters, 35 (19), (1999), p. 1634

[15] Robert Weiss, Reinhard Baumann, *Changing Offset Printing: From Color to Functionality,* Latest Technology & Applications for Printed Electronics- Impact on Printing and Packaging, 21 Jan 2004

[16] Glyn Holland , Peter Harrop, Raghu Das, The A to Z of Printed and Disposal Electronics Terms, April 2005

[17] Peter Harrop, IDTechEx, *Printed Electronics Masterclass* presentation*,* Printed electronics 2004 Printed Electronics 2004, Dec 7 (2004), New Orleans. USA, (http://printedelectronics.idtechex.com/printedelectronics04/en/masterclass.asp)

[18] H. Sirringhaus, T. Kawase, R.H. Friend, T. Shimoda, M. Imbasekaren, W. Wu, E. P. Woo, *High Resolution Inkjet Printing of All-Polymer Transistor Circuits*, Science, 290, (2000), p. 2123

[19] L. Torsi, A. Tafuri, N. Cioffi, M.C. Gallazzi, A. Sassella, L. Sabbatini, P.G. Zambonin*, Regioregular polythiophene field-effect transistors employed as chemical sensors,* Sensors and Actuators*,* B**,** Chemical, 93, (1-3), (Aug 1, 2003), p. 257-262

[20] http://en.wikipedia.org/wiki/Lithography

[21] Jim Parker, *Practical Considerations of Printing Conductive Materials,* IMAPS 3rd Advanced Techology Workshop on Printing an Intellegent Future: Printed Organic and Molecular Electronics Technologies, Annapolis, Maryland, 28-30 September 2004

[22] http://www.p2pays.org/ref/03/02453/flexography.htm

[23] Daniel R. Gamota, Paul Brazis, Krishna Kalyanasundaram, Jie Zhang, *Printed Organic and Molecular Electronics,* Kluwer Academic Publishers (Boston/Dordrecht/New York/London), Springer, March 2004.

[24] http://www.inkworldmagazine.com/Oct033.htm

[25] M Angelopoulos, *Conducting Polymers in Microelectronics,* IBM J. Research and Development, 45 (1), (2001), p. 57

[26] T. R. Hebner, C. C. Wu, D. Marcy, M. H. Lu, and J. C. Sturm, *Ink-jet printing of doped polymers for organic light emitting devices*, Applied Physics Letters, 72 (5), (1998), p. 519-521

[27] G. Yu, A. J. Heeger, *Charge Separation and Photovoltaic Conversion in Polymer Composites with Internal Donor/Acceptor Heterojunctions*, J. Appl. Phys. 78, (1995), p. 4510

[28] A. Assadi, C. Svensson, M. Wilander, O. Inganas, *Field Effect Mobility of Poly(3-hexylthiophene)*, Appl. Phys. Lett. 53 (3), (1988), p. 195

[29] Sung Kyu Park, Yong Hoon Kim, Jeong In Han, Dae Gyu Moon, Won Keun Kim, *High-Performance Polymer TFTs Printed on a Plastic Substrate*, IEEE Transactions on Electron Devices, 49 (11) (2002), p. 2008.

[30] Klaus Dimmler, *Printable, Plastic RFID Tags* presentation, Printed electronics 2004, Dec 7 (2004), New Orleans. USA

[31] Scott Kisting, The Dow Chemical Company, *Materials for Printed Electronics presentation*, Latest Technology & Applications for Printed Electronics - Impact on Printing & Packaging PIRA, Printed Electronics 2004, January 04

[32] Y. Cao, P. Smith, A. J. Heeger, *Counter Ion Induced Processibility of Conducting Polyaniline,* Synthetic Metals 57 (1), (1993), 3514-3519

[33] M. Ahlskog et al, *Heat Induced Transition to the Conducting State in Polyaniline/Dodecylbenzenesulfonic Acid Complex,* Synthetic Metals 69, (1995), p. 213-214

[34] T. Vikki, O. T. Ikkala, *On the Dynamic-Mechanical Relaxation of Polyaniline(Dodecylbenzenesulfonic Acid)-Salt,* Synthetic Metals 69, (1995), p. 235-236

[35] O. T. Ikkala et al, *On The Molecular Recognition and Associations Between Electrically Conducting Polyaniline and Solvents,* J. Chem. Phys, 103 (22), 8 Dec (1995)

[36] Patrick A. McCarthy, Sze C. Yang, *Synthesis of a Water Dispersible Inter-Polymer Complex of Polyaniline,* Materials Research Society Symposium Proceedings, p.598 (2000)

[37] Zhiming Zhang, Zhixiang Wei, Miexiang Wan, *Nanostructures of Polyaniline Doped with Inorganic Acids.* Macromolecules 35, (2000), p. 5937-5942

[38] Jiaxing Huang et al, *Polyaniline Nanofibers: Facile Synthesis and Chemical Sensors,* J. Am. Chem. Soc. 125 (2003), p. 314-315

[39] Jiaxing Huang, Richard Kaner, *Nanofiber Formation in the Chemical Polymerization of Aniline: A Mechanistic Study,* Angew. Chem. Int. Ed. 43, (2004), p. 5817-5821

[40] Yu Xia, *Fabrication of Electronic Devices Using High Volume Printing Techniques,* M. S. Thesis 2005, Rochester Institute of Technology

[41] S. Cichos, J. Haberland, H. Reichl, *Performnce Analysis of Polymer based Antenna-Coils for RFID,* IEEE Polytronic 2002 Conference, p. 120.

[42] Vivek Subramanian, et. al., *Progress Toward Development of All-Printed RFID Tags: Materials, Processes, and Devices*, Proceedings of the IEEE, 93 (7), July (2005), p. 1330.

[43] Jean Roncali, *Conjugated Polythiophenes: Synthesis, Functionalization and Applications,* Chem Rev., 92 (1992), p. 711-738

[44] R. L. Elsenbaumer et. al., *Processible, Environmentally Stable, Highly Conductive Forms of Polythiophene,* Synthetic Metals, 18, (1987), p. 277-282

[45] N. Mermilliod-Thevenin, *One Step Chemical Synthesis and Doping of Poly(2,2-Bithiophene) and Related Polymers,* Mol. Cryst. Liq. Cryst., 118, (1985) p. 227-233

[46] M. Sato, S. Tanaka, K. Kaeriyama, *Soluble Conductive Polythiophenes,* J. Chem. Soc., Chem. Commun., (1989), p. 873

[47] W. R Salaneck, D. T. Clark, E. J. Samuelsen, *Science and Applications of Conducting Polymers,* 6th European Physical Society Industrial Workshop – Lofthus, Norway 1990*,* Adam Hilger, Bristol, Philidelphia, New York p.181

[48] T. W. Smith, et. al, *Processible Environmentally Stable Conducting Polymer Composites,* Polymer Preprints, 39, 1, (1998), p. 58

[49] U.S. Patent: 6,605,236, Thomas W. Smith, David J. Luca.

[50] George Odian, *Principles of Polymerization, 4th Edition,* John Wiley & Sons, Inc., Publication, p. 287

[51] A. K. Srivastava et. al., *Studies on Template Polymerization,* J. Macromol. Sci. – Rev. Macromol. Chem. Phys., C27(2), (1986), p. 171-180

[52] S. Klingelhofer, W Heitz, A. Greiner, S. Oestreich, S. Forster, M. Antonietti, *Preparation of Palladium Colloids in Block Copolymer Micelles and Their Use for* the Catalysis of the Heck Reaction, J. Ame. Chem. Soc. 119 (1997) p. 10116

[53] L. Bronstein, E Kramer, B. Berton, C. Burger, S. Forster, M. Antonietti, *Successive Use of Amphiphilic Block Copolymers as Nanoreactors and Templates: Preparation of Porous Silica with Metal Nanoparticles*, Chem. Mat. 11, (1999), p. 1402

[54] Stephan Forster, *Amphiphillic Block Copolymers for Templating Applications,* Topics in Current Chemistry, 226, (2003), p. 1-28

[55] A. Mohammadi, et. al., *Electrically Conductive Composites Prepared by Template Polymerization of Pyrrole into a Complexed Polymer,* J. of Polymer Science, Part A, Polymer Chemistry, 32, (1994), p. 495-502

[56] F. S. Bates, G. H. Fredrickson, *Block Copolymer Thermodynamics: Theory and Experiment,* Annu. Rev. Phys. Chem. 41, (1990), p. 525-557

[57] G. Carrot. et. al, *Gold Nanoparticle Synthesis in Graft Copolymer Micelles,* Colloid Polym. Sci., 276, (1998), p. 853-859

[58] M. D. Whitemore, T. W. Smith, *Swelling of Coplymer Micelles by Adding Homopolymer,* Macromolecules, 27, (1994), p. 4673-4683

[59] John Coates, *Interpretation of Infrared Spectra, A Practical Approach,* Encyclopedia of Analytical Chemistry, R.A. Meyers (Ed.), (2000), Ó John Wiley & Sons Ltd, Chichester, p. 10815–10837

[60] Nicholas A. Peppas, et. al., *Preparation and Properties of Poly(ethylene oxide) Star Polymers,* J. App. Poly. Sci., 87, (2003), p. 322-327

[61] G. Louran, J. P. Buisson, S. Lefrant, *Vibrational Studiesof a Series of α-Oligothiophenes as Model Systems of Polythiophene,* J. Phys. Chem. 99, (1995), p. 11399-11404

[62] Li Zhi-Weia, Zhou Jing-Fanga, Zhang Zhi-Jun, Dang Hong-Xina, *Self-assembly of Carboxyl Functionalized Polystyrene Nanospheres into Close-packed Monolayers via Chemical Adsorption,* Chinese Journal of Chemistry, 22, (2004), p. 1133 1137

[63] Shenglong Wang, Kazuyoshi Tanaka, Tokio Yamabe, *A Study of the Electroactivity Decay of Polythiophene Film Electrodes,* Synthetic Metals, 32, (1989), p. 141-150

[64] Linhai Yue, Dalai Jin, Miao Shui, Zhude Xu, *Study on the Synthesis of Spherulitic Calcium Carbonate Composite in Amphiphilic PS-b-PAA Solution and its Crystalline Structure,* Solid State Sciences, 6, (2004), p.1007–1012